

Received 20 June 2022, accepted 20 July 2022, date of publication 25 July 2022, date of current version 28 July 2022.

Digital Object Identifier 10.1109/ACCESS.2022.3193371

RESEARCH ARTICLE

Multiobjective Optimal Power Flow Using Multiobjective Search Group Algorithm

TRUONG HOANG BAO HUY^{ID1}, DAEHEE KIM^{ID1}, (Member, IEEE), AND DIEU NGOC VO^{ID2,3}

¹Department of Future Convergence Technology, Soochunhyang University, Asan 31538, South Korea

²Department of Power Systems, Ho Chi Minh City University of Technology (HCMUT), Ho Chi Minh City 72506, Vietnam

³Vietnam National University Ho Chi Minh City (VNU-HCM), Ho Chi Minh City 71308, Vietnam

Corresponding authors: Daehee Kim (daeheekim@sch.ac.kr) and Dieu Ngoc Vo (vndieu@hcmut.edu.vn)

This work was supported in part by the Korea Institute of Energy Technology Evaluation and Planning (KETEP) and the Ministry of Trade, Industry and Energy (MOTIE), Republic of Korea, under Grant 20184030202130; and in part by the Soonchunhyang University Research Fund.

ABSTRACT This paper proposes a new multi-objective method that efficiently solves the multi-objective optimal power flow (MOOPF) problem in power systems. The objective of solving the MOOPF problem is to concurrently optimize the fuel cost, emissions, and active power loss. The proposed multi-objective search group algorithm (MOSGA) is an effective method that combines the merits of the original search group algorithm with fast nondominated sorting, crowding distance, and archive selection strategies to acquire a nondominated set in a single run. The MOSGA is employed on IEEE 30-bus and 57-bus systems to validate its robustness and efficiency. It was found that implementing MOSGA to solve the MOOPF significantly enhanced the performance of power systems in terms of economic, environmental, and technical benefits. As for Case 6, the fuel cost, emissions, and active power loss were reduced by 16.5707%, 52.0605%, and 60.9443%, respectively. The simulation results were analyzed and compared with those of previously reported studies based on the best individual solutions, compromise solutions, and performance indicators. The comparative results confirmed the potential and advantage of MOSGA when solving the MOOPF problem efficiently and MOSGA had high-quality optimal solutions.

INDEX TERMS Multi-objective search group algorithm, multi-objective optimal power flow, fuel cost, emissions.

I. INTRODUCTION

Optimal power flow (OPF) is a critical optimization problem in modern power systems [1]. The OPF problem seeks a steady-state operation point of generators so that a specific objective is optimized while satisfying various operational constraints, such as the power flow balance, voltage, active and reactive power outputs of the generators, shunt compensators, transformer tap setting, voltage magnitude at load bus, and transmission line loading [2]. OPF is generally a nonconvex, nonlinear, mixed-integer, highly constrained, and large-scale optimization problem [3], [4]. While the primary objective of the traditional OPF solution is to minimize fuel costs, utilities have commercial concerns, and it is necessary

to reduce transmission losses to maintain a high level of power quality. Moreover, growing environmental concerns require the consideration of emission levels as an objective function rather than a constraint [5]. Therefore, a multi-objective OPF (MOOPF) was developed to address multiple objective functions, namely the fuel cost, emissions, and active power loss.

The MOOPF problem has been the subject of extensive research over the past few years, and various meta-heuristic algorithms have been successfully used to address the MOOPF problem. The two most common approaches are classical methods and multi-objective evolutionary algorithms (MOEAs). Traditional methods transform a multi-objective problem into a single-objective problem by designating a suitable weighting factor for each objective. Some of the latest traditional methods include the

The associate editor coordinating the review of this manuscript and approving it for publication was Mauro Tucci^{ID}.

backtracking search optimization algorithm (BSA) [1], black hole (BH) [6], artificial bee colony (ABC) [7], improved colliding bodies optimizer (ICBO) [8], enhanced ant colony optimization (EACO) [9], moth-swarm algorithm (MSA) [10], differential search algorithm (DSA) [11], differential evolution (DE) [12], and improved moth-flame optimization (IMFO) [13]. These approaches are easy to implement and can use single-objective algorithms directly without modification. However, they could only obtain an optimal solution in one simulation run of the algorithm. Hence, these methods cannot identify the trade-offs between multiple objectives.

In recent years, several novel and effective MOEAs have been adopted to address the MOOPF problem. These methods aim to provide an accurate depiction of the Pareto optimal front and offer a broader range of solutions for decision makers. An example is the modified shuffle frog leap algorithm (MSFLA) [14], which has been proposed for a 30-bus system. In [15], the teaching learning-based optimization (TLBO) was integrated with a quasi-opposition approach to boost the solution's quality and convergence speed. The TLBO method was applied to optimize the power losses, voltage stability index, fuel cost, and emissions. In [16], the authors recommended a modified TLBO (MTLBO) to handle the MOOPF problem with emission and cost objectives. Bilel *et al.* [17] studied the MOOPF problem for 33-bus and Algerian 59-bus systems using a multiple objective imperialism competition algorithm (MOICA). In [18], the OPF concept was applied to bidirectional photovoltaics and batteries in the microgrid. In [19], the authors modified a multiple objective multihive bee algorithm (MHBA) by integrating an external archive to solve the MOOPF problem. A comprehensive learning method was used to determine the flight behavior of bees. Greedy selection and crowding distance techniques were used to maintain nondominated solutions in an archive. Zhang *et al.* [20] introduced an MOEA-based decomposition (MOEA/D) to handle the MOOPF. The fuel cost, voltage deviations, power losses, and emissions were chosen for seven scenarios on a 30-bus system. A modified decomposition algorithm was integrated with a decision-making method and a mixed constraint-handling technique. MOEA/D was compared with other methods based on different performance indicators and was shown to have excellent performance and yield competitive solutions. A modified Gaussian bare-bones imperialism competition algorithm (MGBICA) was developed in [21] to determine the optimal electric power planning strategy. To overwhelmed the difficulty of tuning the control parameters, the authors in [22] established an enhanced self-adaptive DE and a mix crossover operator (ESDE-MC) to handle single- and MOOPF problems. In [23], the improved strength of Pareto evolutionary algorithm 2 (ISPEA2) was assessed on 30- and 57-bus networks for the MOOPF problem. Warid *et al.* [24] provided a solution to the MOOPF problem through a quasi-opposite modified Jaya (QOMJaya) algorithm and validated it on a 30-bus network. The exploration capability of the QOMJaya was improved by integrating a quasioppositional approach. In [25], the MOOPF

problem was solved using a multiple objective dimension-based firefly algorithm (MODFA), which was employed on 30- and 57-bus networks in nine case studies. In [26], a hybrid DE was implemented along with a harmony search (HS) for the MOOPF solution. In addition to the voltages and real power of the generator buses, transformer tap settings and reactive power compensators were included in the control variables; 30-, 118-, and 300-bus networks were used to verify the usefulness of the proposed method. Zhang *et al.* [27] enhanced the nondominated sorting genetic algorithm III (NSGA-III) to minimize numerous OPF objectives, namely emissions, fuel costs, voltage magnitude deviations, line indexes, and active power losses. In [28], the authors suggested a combination of particle swarm optimization (PSO) and salp swarm optimizer (SSO) methods to solve the MOOPF issue. Biswas *et al.* [29] implemented the MOEA/D method, integrating the benefits of feasible solutions (SF) into MOEA/D to address the restrictions of the MOOPF. The MOEA/D-SF was tested on 30- and 57-bus networks. A modified pigeon-inspired optimization combined with a constraint-objective sorting rule (MPIO-COSR) was introduced by Chen *et al.* [30] to deal with the MOOPF considering three separate objective functions: emissions, fuel costs with valve-point effects, and active power losses. The case studies performed by Chen *et al.* [30] were repeated in [31] using a multi-object beetle antennae search (NMBAS), in [32] using a hybrid bat algorithm with constrained Pareto fuzzy dominance (NHBA-CPFD), and in [33] using a hybrid firefly-bat algorithm with a constraint-prior object-fuzzy sorting strategy (HFBA-COFS). In [34], the OPF and MOOPF problems were solved by using joint self-adaptive PSO and differential evolution (FAHSPSO-DE). This study considered active power loss, fuel costs, and emissions as three objective functions. Shaheen *et al.* [35] developed a multi-objective quasi-reflected jellyfish search optimization (MOQRJFS) to address the MOOPF problem. The authors validated the performance of MOQRJFS on 30-bus, 57-bus, and practical power networks in Egypt. It was concluded that MOQRJFS was better than the original MOJFS. In [36], the authors integrated an effective exploitation feature to develop an improved heap-based optimizer algorithm (IHOA) to deal with the MOOPF problem. The improved exploitation approach helps the IHOA to increase the search for the best solutions and avoid local trapping. To handle the MOOPF problem, Qian *et al.* [37] suggested a modified hybrid beetle antennae search (MHBAS) method with an adaptively-adjusted step factor. The authors indicated that MHBAS was better than NSGA-II and multi-objective differential evolution (MDE) for solution quality and computational cost. For dealing with the MOOPF problem with different objectives, Kahraman *et al.* [38] developed an improved multiple objective manta ray foraging optimizer (IMOMRFO) based on a Pareto strategy and crowding distance method.

As can be seen from the literature review, MOEAs have been widely used for solving MOOPF problems. They offer decision makers a variety of trade-off solutions in one

simulation run. However, because MOOPF requires complex and large-scale optimization, no algorithm can effectively optimize all of the problems. Hence, new or improved MOEAs can be developed to find more efficient solutions to MOOPF problems. Moreover, most previous studies evaluated the performance of algorithms based on the best compromise solutions and Pareto optimal fronts. The efficiency of MOEAs in solving the MOOPF problem should be thoroughly evaluated based on two crucial criteria, convergence and distribution, using performance indicators such as spread and hypervolume metrics. This requires us to offer a new multi-objective method for generating Pareto optimal solutions for the MOOPF.

This study aimed to develop and apply a new multi-objective search group algorithm (MOSGA) to handle the MOOPF problem formulated with fuel cost, emissions, and active power loss objective functions. The control variables of the problem include the real power output of the thermal generator, voltage magnitude at generation bus, transformer tap setting, and shunt VAR compensation. To develop the MOSGA, archive selection, fast nondominated sorting, and crowding distance strategies were combined with the original SGA. The MOSGA was proposed to generate a Pareto front with high convergence and diversity for the MOOPF solution. The efficacy of the proposed MOSGA was verified in IEEE 30- and 57-bus systems. It was found that implementing the MOSGA to handle the MOOPF problem resulted in improved performance in power systems compared to the initial metrics. Furthermore, the simulation results achieved by the MOSGA were compared with those achieved by the nondominated sorting genetic algorithm II (NSGA-II), multi-objective ant lion optimizer (MOALO), multi-objective grasshopper optimization algorithm (MOGOA), and other previous studies in the literature. The comparisons were conducted based on the optimal results of compromise solution, spread metric, and hypervolume metric, which showed that the MOSGA outperformed these approaches regarding solution quality.

The rest of this study is organized as follows. The MOOPF problem is formulated in Section II. Section III describes the proposed MOSGA and its implementation. Section IV gives the simulation results. Section V presents the conclusion of this study.

II. PROBLEM FORMULATION

The primary purpose of the MOOPF problem is to identify the optimal control variables to optimize various objective functions; inequality and equality constraints must also be satisfied concurrently. The MOOPF problem is expressed as follows [39]:

$$\text{Minimize : } F(u, x) = [F_1(u, x), F_2(u, x), \dots, F_m(u, x)] \quad (1)$$

$$\text{Subject to : } g(u, x) \leq 0 \quad (2)$$

$$h(u, x) = 0 \quad (3)$$

where u denotes the set of independent and control variables, x signifies the set of dependent/state variables, $F(u, x)$ represents the set of objective functions to be optimized, and $g(x, u)$ and $h(x, u)$ refer to inequality and equality constraints, respectively.

A. OBJECTIVE FUNCTIONS

The MOOPF problem considers three objectives that reflect the economic, environmental, and technical factors, as described below.

1) FUEL COST

The fuel cost of power generation is formulated using a quadratic function as follows [1], [10]:

$$F_1 = \sum_{i=1}^{NG} (a_i + b_i P_{G,i} + c_i P_{G,i}^2) \quad (4)$$

where NG indicates the number of generators, $P_{G,i}$ refers to the active power output of the i^{th} generator, and a_i , b_i , and c_i denote the cost coefficients of the i^{th} generator.

2) EMISSIONS

Atmospheric pollutants are released during the generation of electricity by thermal units using fossil fuels. The total emissions (ton/h) of harmful gases are determined by the following equation [40]:

$$F_2 = \sum_{i=1}^{NG} \left[(\alpha_i + \beta_i P_{G,i} + \gamma_i P_{G,i}^2) + \omega_i e^{(\mu_i P_{G,i})} \right] \quad (5)$$

where α_i , β_i , γ_i , ω_i , and μ_i are the emission characteristics of the i^{th} generator.

3) ACTIVE POWER LOSS

Power loss in power systems is inevitable because transmission lines possess built-in resistances. The active power loss is obtained as follows [10]:

$$F_3 = P_L = \sum_{q=1}^{NL} G_{q(ij)} \left[V_i^2 + V_j^2 - 2V_i V_j \cos(\theta_i - \theta_j) \right] \quad (6)$$

where V_i and θ_i symbolize voltage magnitude and voltage angle at bus i , respectively, $G_{q(ij)}$ represents the transfer conductance between bus i and bus j , and NL symbolizes the number of transmission lines.

B. CONTROL VARIABLES

The vector of control variables is signified by the following equation [1]:

$$u = [P_{G,2}, \dots, P_{G,NG}, V_{G,1}, \dots, V_{G,NG}, Q_{C,1}, \dots, Q_{C,NC}, T_1, \dots, T_{NT}]^T \quad (7)$$

where P_G , V_G , Q_C , and T denote the active power outputs at the generation buses (PV buses) except the slack bus, voltage magnitudes at the generation buses, shunt VAR compensations, and transformer tap settings, respectively, NC

symbolizes the number of shunt VAR compensators, and NT symbolizes the number of transformer tap settings.

C. STATE VARIABLES

The vector of state variables can be defined in the following equation [1]:

$$\mathbf{x} = [P_{G,1}, V_{L,1}, \dots, V_{L,ND}, Q_{G,1}, \dots, Q_{G,NG}, S_{L,1}, \dots, S_{L,NL}]^T \quad (8)$$

where P_{G1} , V_L , Q_G , and S_L denote the active power output at the slack bus, voltage magnitudes at the load buses (PQ buses), reactive power outputs of the generators, and transmission line loadings, respectively, ND is the number of load buses.

D. CONSTRAINTS

1) EQUALITY CONSTRAINTS

The equality constraints represent nonlinear power flow equations that control power systems as follows [6]:

$$P_{G,i} - P_{D,i} = V_i \sum_{j=1}^{NB} V_j [G_{ij} \cos(\theta_i - \theta_j) + B_{ij} \sin(\theta_i - \theta_j)] \quad i = 1, \dots, NB \quad (9)$$

$$Q_{G,i} - Q_{D,i} = V_i \sum_{j=1}^{NB} V_j [G_{ij} \cos(\theta_i - \theta_j) - B_{ij} \sin(\theta_i - \theta_j)] \quad i = 1, \dots, NB \quad (10)$$

where $P_{D,i}$ and $Q_{D,i}$ respectively signify the active and reactive load demands, B_{ij} and G_{ij} denote the transfer susceptance and conductance between buses i and j , respectively, and NB symbolizes the number of buses.

2) INEQUALITY CONSTRAINTS

The inequality constraints describe operating limits of power systems to guarantee system security:

Generator constraints: The voltage and the active and reactive power outputs of the generators must be bounded by the specified restrictions [8]:

$$V_{G,i}^{\min} \leq V_{G,i} \leq V_{G,i}^{\max}; \quad i = 1, \dots, NG \quad (11)$$

$$P_{G,i}^{\min} \leq P_{G,i} \leq P_{G,i}^{\max}; \quad i = 1, \dots, NG \quad (12)$$

$$Q_{G,i}^{\min} \leq Q_{G,i} \leq Q_{G,i}^{\max}; \quad i = 1, \dots, NG \quad (13)$$

Shunt VAR compensator constraints: The restrictions of the shunt VAR compensators must be set as follows [8]:

$$Q_{C,i}^{\min} \leq Q_{C,i} \leq Q_{C,i}^{\max}; \quad i = 1, \dots, NC \quad (14)$$

Transformer constraints: The tap settings of the transformers must be limited within their boundaries as follows [12]:

$$T_i^{\min} \leq T_i \leq T_i^{\max}; \quad i = 1, \dots, NT \quad (15)$$

Security constraints: The limitations of the transmission line loading and voltage magnitude at the load buses can be

formulated in the following constraints [12]:

$$S_{L,i} \leq S_{L,i}^{\max}; \quad i = 1, \dots, NL \quad (16)$$

$$V_{L,i}^{\min} \leq V_{L,i} \leq V_{L,i}^{\max}; \quad i = 1, \dots, ND \quad (17)$$

III. MULTI-OBJECTIVE SEARCH GROUP ALGORITHM

The proposed MOSGA was developed by incorporating three schemes: crowding distance, fast nondominated sorting, and archive selection. The conventional SGA [41] and the proposed MOSGA are introduced in the following subsections.

A. SGA

1) INITIAL POPULATION

In the search domain, population \mathbf{P} is randomly created to start the optimization process as follows [41]:

$$P_{ij} = X_{j,\min} + (X_{j,\max} - X_{j,\min})U[0, 1]; \\ i = 1, \dots, n_{pop}, \quad j = 1, \dots, n, \quad (18)$$

where P_{ij} symbolizes the j^{th} control variable of the i^{th} individual of \mathbf{P} , $X_{j,\min}$ and $X_{j,\max}$ refer to the limitations of the j^{th} control variable, n signifies the number of control variables, n_{pop} denotes the population size, and $U[0,1]$ is the uniform distribution.

2) SELECTION OF THE INITIAL SEARCH GROUP

The objective function values are computed for all individuals from \mathbf{P} once the initial population is established. From \mathbf{P} , a search group \mathbf{R} with n_g members is formed. The selection process includes a tournament in which the best individuals are randomly selected from a chosen subgroup. Further information about the tournament selection can be found in [42]. At each iteration, the members of the search group \mathbf{R} are sorted based on their objective function values.

3) SEARCH GROUP MUTATION

At each iteration, the members of the search group \mathbf{R} can be mutated to boost the algorithm's global searchability. The n_{mut} members from \mathbf{R} are replaced by new individuals, depending on the statistics of the current search group in this mutation strategy. The aim is to create new members in positions that are different from those of the current members, allowing the algorithm to explore new regions of the design domain. Consequently, new individuals can be created in the following manner [41], [43]:

$$X_{j,mut} = E[R_{:,j}] + t\sigma[R_{:,j}]; \quad j = 1, \dots, n, \quad (19)$$

where $X_{j,mut}$ denotes the j^{th} control variable of a mutated member, E and σ represent the mean value and standard deviation operators, ε symbolizes a random number, t signifies a parameter controlling how far away a new member can be created, and $R_{:,j}$ represents the j^{th} column of the search group matrix. The likelihood of the members being mutated is linked to their rank in the current search group. In other words, they are more likely to replace the worst individuals. An inverse tournament selection is used to accomplish this

process, and this is a variation of the selection procedure outlined in Section III.A.2. Here, the worst individuals are replaced by new individuals by adopting Eq. (19).

Algorithm 1: Pseudocode of SG.A

- 1: Initialize the initial parameters of SGA;
- 2: Generate the initial population \mathbf{P} using Eq. (18);
- 3: Evaluate objective function value for each individual in the initial population \mathbf{P} ;
- 4: Create the initial search group \mathbf{R}^k selecting n_g individuals from the initial population;
- 5: Replace n_{mut} individuals by new members created as described in Eq. (19);
- 6: Generate the families \mathbf{F}_i using Eq. (20);
- 7: Select the new search group according to the rule:
 - Global phase: search group \mathbf{R}^{k+1} is formed by the best member of each family;
 - Local phase: search group \mathbf{R}^{k+1} is formed by the best n_g individuals from Pareto archive.
- 8: Update α^{k+1} accordingly to Eq. (21);
- 9: Make $k = k + 1$, if $k > Iter_{max}$ go to Step 10, otherwise return to Step 5;
- 10: Solution found: $\mathbf{x}^* = \mathbf{R}_1, \dots$

4) GENERATION OF FAMILIES FOR EACH MEMBER OF SEARCH GROUP

Families are formed during this phase. A family includes a search group member and individuals created by this search group member. \mathbf{F}_i denotes each family with $i = 1 - n_g$. Therefore, each member in the search group creates a family as follows [41], [43]:

$$X_{j,\text{new}} = R_{ij} + \alpha \varepsilon; \quad j = 1, \dots, n, \quad (20)$$

where α regulates the perturbation size. This parameter decrements over iterations of the search procedure. The update of α value at $(k+1)^{\text{th}}$ iteration can be expressed as:

$$\alpha^{k+1} = b\alpha^k \quad (21)$$

where b denotes an SGA parameter.

It should be noted that the variation in α^k determines how the search is to be performed. In the early iterations, it is designed to allow any individual to visit any region in the search space in a probabilistic sense; this highlights the importance of exploration. The value of α^k decreases as the iterations progress. The search procedure narrows its scope in favor of a more concentrated search of the promising areas discovered. To avoid a null diversification value, parameter α^{\min} is defined, which is the lower limit of α .

Another significant feature of this approach is the size of the family; this can also mean that the number of individuals generated by a search group member can change depending on their performance. Individuals with lower objective values have larger families than those with higher objective values. The vector v is responsible for this feature, and it has the same number of elements as the search group. The number of individuals in the i^{th} search group corresponds to the i^{th} value of the vector v . To set up the proposed algorithm, two principles must be followed: (i) $\sum(v) = n_{pop} - n_g$ and (ii) $v^{i+1} \leq v^i$. The first principle aims to keep the number of individuals constant at iterations, and the second is to allow better individuals to create larger families.

5) SELECTION OF THE NEW SEARCH GROUP

The proposed method consists of two phases: local and global. The primary goal of the algorithm during the initial iterations is to explore the majority of the search domain, which is the global phase. Thus, the best member of each family is the next search group member. The selection strategy is altered when the iteration number exceeds $Iter_{global,max}$, and the best n_g individuals from all of the families generate a new search group. In this local phase, the algorithm tends to exploit regions of the most recent best design. Algorithm 1 describes the pseudocode of SGA.

B. FAST NONDominated SORTING AND CROWDING DISTANCE STRATEGIES

Because a multi-objective problem contains more than one objective function, it is not possible to sort individuals in a population based on their objective function values. To obtain uniformly distributed nondominated solutions, crowding distance computations and fast nondominated sorting [44] are employed to create a ranking method for solutions in a multiobjective space.

Algorithm 2: Pseudocode of MOSGA

- 1: Initialize the parameters of MOSGA;
- 2: Randomly Generate the initial population \mathbf{P} using Eq. (18);
- 3: Evaluate multiple objective function values for each individual in the initial population \mathbf{P} ;
- 4: Sort initial population \mathbf{P} based on fast non-dominated sorting and crowding distance techniques and store them in the Pareto archive;
- 5: Create the initial search group \mathbf{R}^k selecting n_g individuals from the initial population;
- 6: Replace n_{mut} individuals by new members created as described in Eq. (19);
- 7: Generate the families \mathbf{F}_i , using Eq. (20);
- 8: Store all newly created individuals in the advanced Pareto archive. Combine the current and advanced archives;
- 9: Select the best solutions for new Pareto archive using Pareto archive selection mechanism;
- 10: Select the new search group according to the rule:
 - Global phase: search group \mathbf{R}^{k+1} is formed by the best member of each family;
 - Local phase: search group \mathbf{R}^{k+1} is formed by best n_g individuals from Pareto archive;
- 11: Update α^{k+1} accordingly to Eq. (21);
- 12: Make $k = k + 1$, if $k > Iter_{max}$, go to Step 13, otherwise return to Step 6;
- 13: Solution found: Pareto optimal solutions in the last Pareto archive.

In a fast nondominated sorting approach, two criteria are identified for all of the solutions in the population: 1) dominated count n_i , which is the number of solutions that dominate solution i , and 2) S_i , which is a set of solutions dominated by solution i . The first nondominated front includes all solutions with a dominated count n_i of zero. Then, we consider each member (j) of set S_j and decrease its dominated count by one for each solution i with $n_i = 0$. Subsequently, any member j with a dominated count of zero is placed in a separate list J (second nondominated front). This method is repeated for each member of J until the third front is discovered. This procedure is continued until all fronts are determined. The fast nondominated sorting method is shown schematically in Fig. 1.

The density of solutions surrounding a specific solution is then estimated by a crowding distance computation that determines for each objective the average distance to two points on each side. This method sorts the objective function values in the population in ascending order. An infinite

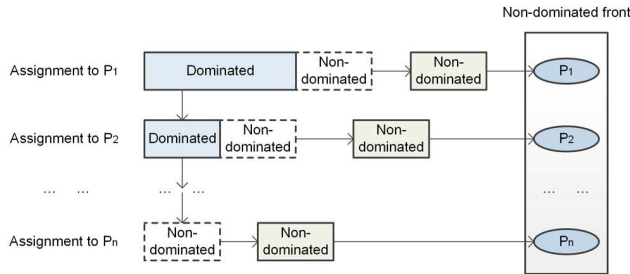


FIGURE 1. Diagrammatic perspective of fast nondominated sorting approach.

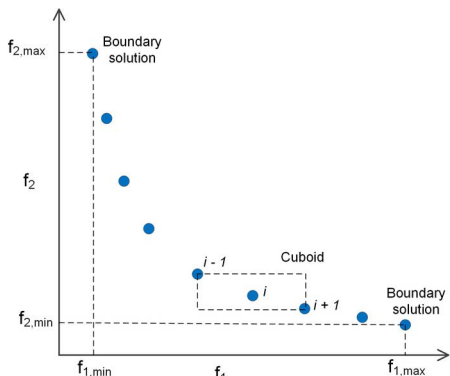


FIGURE 2. Simplified visualization of crowding-distance computation.

distance value is assigned to the solutions with the lowest and highest function values for each objective (i.e., boundary solutions). For all other intermediate solutions, a distance value that equals the absolute normalized difference in the function values of two neighboring solutions is calculated as follows [44], [45]:

$$d_{ij} = \sum_{j=1}^{n_{obj}} \frac{f_{(i+1),j} - f_{(i-1),j}}{f_{j,\max} - f_{j,\min}} \quad (22)$$

where n_{obj} denotes the number of objectives; $f_{(i+1),j}$ and $f_{(i-1),j}$ respectively signify the j^{th} objective values for the two neighboring solutions of solution i , $f_{j,\max}$ and $f_{j,\min}$ respectively indicate the largest and smallest values of the j^{th} objective. Solutions located in less crowded areas have greater crowding distance values than the other solutions. Fig. 2 shows the crowding distance computation.

After the crowding distance and fast nondominated sorting approaches have been completed, each individual has two qualities: crowding distance (cd) and nondominated rank (r). To obtain a uniformly spread Pareto optimal front, the crowded-comparison operator (\prec_n) is used to compare the two solutions in a multi-objective space as follows [44], [45]:

$$i \prec_n j \text{ if } (r_i < r_j) \text{ or } ((r_i = r_j) \text{ and } (cd_i > cd_j)) \quad (23)$$

When two solutions are in different nondominated ranks, the solution with the best rank is preferred. Otherwise, if both solutions are of the same rank, a solution with a higher

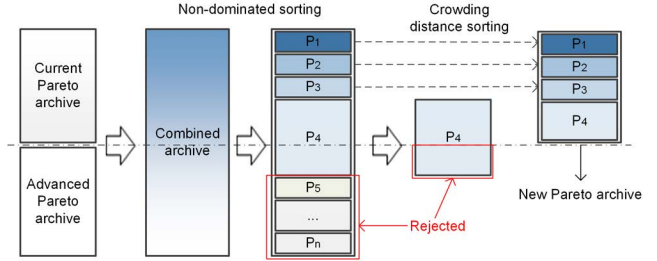


FIGURE 3. Diagrammatic perspective of pareto archive selection.

crowding distance value is preferred. Hence, the crowded-comparison operator provides a ranking method to sort individuals in a multi-objective space.

C. PARETO ARCHIVE SELECTION

To conduct multi-objective optimization, a Pareto archive of size N_Ω stores the nondominated solutions. A selection strategy is employed at every iteration to update the archive and to prevent the loss of promising solutions [44]. Fig. 3 outlines the selection strategy. In the proposed MOSGA, all of the newly produced solutions are included in an advanced archive. At the end of the generation, the advanced and current archives are combined. The size of the combined set exceeds the size limit of the archive; thus, the archive is truncated by discarding undesirable solutions. All solutions in the combined archive are ranked using crowding distance computations and fast nondominated sorting. Subsequently, the best N_Ω solutions from the combined archive corresponding to the best nondominated ranks and crowding distance values are selected as the new Pareto archive.

D. THE PROPOSED MOSGA

The MOSGA begins optimization by establishing a population \mathbf{P} of n_{pop} individuals. Objective value is then computed for each individual within \mathbf{P} . From \mathbf{P} , the n_g best individuals are selected to generate a search group \mathbf{R} based on a tournament selection. The MOSGA then implements two stages: mutation and generation of families. After these two stages, an advanced archive set is obtained and merged with the current archive. The archive selection strategy is executed to define the best N_Ω solutions for the new archive set. The final process is to define a new search group via global and local phases. On the global phase, a new search group is generated from the best members of each family. Then, in the local phase, a new search group is generated from the best n_g individuals in the new archive set. The optimization process of the MOSGA continues until the stop criterion is satisfied. The MOSGA pseudocode is shown in Algorithm 2.

E. APPLICATION OF MOSGA TO MOOPF PROBLEM

1) INITIALIZATION OF POPULATION

To deploy MOSGA for the MOOPF problem, the control variables constitute individuals of the initial population \mathbf{P} . From Eq. (7), the size of the control variable is defined as

follows:

$$n = 2NG + NC + NT - 1 \quad (24)$$

The position of the i^{th} individual comprising n control variables can be expressed as:

$$\begin{aligned} P_i &= [X_{i1}, X_{i2}, \dots, X_{in}] = [P_{iG,1}, \dots, P_{iG,NG}, \\ &\quad V_{iG,1}, \dots, V_{iG,NG}, Q_{iC,1}, \dots, Q_{iC,NC}, \\ &\quad T_{i,1}, \dots, T_{i,NT}]^T; \quad i = 1, \dots, n_{\text{pop}} \end{aligned} \quad (25)$$

In a population with n_{pop} individuals, the population matrix \mathbf{P} is created using Eq. (18) as follows:

$$P = \begin{bmatrix} X_{11} & X_{12} & \dots & X_{1n} \\ X_{21} & X_{22} & \dots & X_{2n} \\ \vdots & \vdots & \ddots & \vdots \\ X_{n_{\text{pop}}1} & X_{n_{\text{pop}}2} & \dots & X_{n_{\text{pop}}n} \end{bmatrix} \quad (26)$$

2) OBJECTIVE FUNCTION VALUE

The objective function values can be defined using the following equation:

$$\begin{aligned} F'_m &= F_m + \lambda_P (P_{G,1} - P_{G,1}^{\lim})^2 + \lambda_Q \sum_{i=1}^{NG} (Q_{G,i} - Q_{G,i}^{\lim})^2 \\ &\quad + \lambda_V \sum_{i=1}^{ND} (V_{L,i} - V_{L,i}^{\lim})^2 + \lambda_S \sum_{i=1}^{NL} (S_{L,i} - S_{L,i}^{\max})^2 \end{aligned} \quad (27)$$

where F_m symbolizes the m^{th} objective of the MOOPF problem, λ_P , λ_Q , λ_V , and λ_S are the penalty coefficients for the inequality constraints of the state variables, namely active power output at the slack bus, reactive power output at generation bus, voltage magnitude at the load bus, and line loading. These penalty coefficients are set at high values to maintain the state variables within tolerable limits and to eliminate infeasible solutions [46]. Further, x^{\lim} denotes the violation limit value of the dependent variable x as follows:

$$x^{\lim} = \begin{cases} x_{\max} & \text{if } x > x_{\max} \\ x_{\min} & \text{if } x < x_{\min} \end{cases} \quad (28)$$

3) BEST COMPROMISE SOLUTION

To make decisions, it is vital to define the best compromise solution after obtaining the Pareto-optimal set. In this study, this solution is identified from the trade-off curve using fuzzy set theory. First, each objective of the i^{th} solution can be defined using the membership function μ_{ij} , which is expressed as follows [47]:

$$\mu_{ij} = \begin{cases} 1 & \text{if } f_{ij} \leq f_{j,\min} \\ \frac{f_{j,\max} - f_{ij}}{f_{j,\max} - f_{j,\min}} & \text{if } f_{j,\min} \leq f_{ij} \leq f_{j,\max} \\ 0 & \text{if } f_{ij} \geq f_{j,\max} \end{cases} \quad (29)$$

where $f_{j,\min}$ and $f_{j,\max}$ respectively denote the maximum and minimum of the j^{th} objective. A diagram of the fuzzy membership function is shown in Fig. 4.

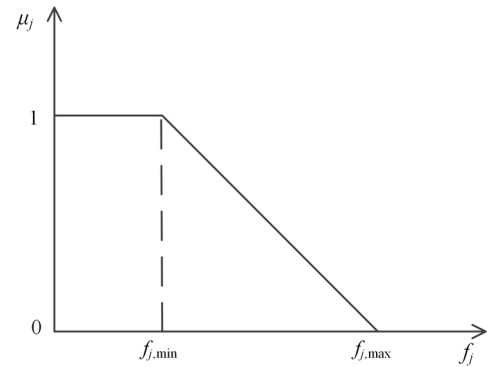


FIGURE 4. Fuzzy membership function.

A higher membership function indicates that the solution achieves greater satisfaction than other solutions. The normalized membership function for each nondominated solution can be then written in the following equation [45]:

$$\mu_i = \frac{\sum_{j=1}^{n_{\text{obj}}} \mu_{ij}}{\sum_{i=1}^{n_{\text{pf}}} \sum_{j=1}^{n_{\text{obj}}} \mu_{ij}} \quad (30)$$

where n_{pf} is the number of nondominated solutions. The best compromise solution is the one with the largest normalized membership function value (μ_i).

4) OVERALL PROCEDURE

The overall procedure of MOSGA application to handle the MOOPF problem can be summarized in the next steps:

Step 1: Define data of the power test systems, fuel cost and emissions coefficients, and the allowed limit of the control variables.

Step 2: Choose MOSGA control parameters, namely the population size (n_{pop}), number of search group members (n_g), number of mutations (n_{mut}), perturbation size (α), Pareto archive size (N_{Ω}), maximum number of iterations of the global phase ($\text{Iter}_{\text{global},\max}$), and the maximum number of iterations (Iter_{\max}).

Step 3: Create the initial population \mathbf{P} of n_{pop} individuals for the control variables within their limits, as described in Section III.E.1.

Step 4: Perform the power flow based on Matpower 6.0 to estimate the objective values (F_1, F_2, F_3) for individuals of \mathbf{P} according to Eq. (27).

Step 5: Sort all individuals of \mathbf{P} based on fast nondominated sorting and crowding distance, and put these individuals into an archive.

Step 6: Define the initial search group \mathbf{R}^k by selecting the best n_g solutions from \mathbf{P} . Set $i = 0$.

Step 7: Set $i = i + 1$.

Step 8: Accomplish the mutation stage for n_{mut} members according to Eq. (19).

TABLE 1. Defining features of IEEE 30-bus and 57-bus systems.

System characteristics	IEEE 30-bus system		IEEE 57-bus system	
	Value	Details	Value	Details
Bus	30	[48]	57	[49]
Branch	41	[48]	80	[49]
Generators	3	Buses: 1, 2, 8	4	Buses: 1, 2, 3, 6, 8, 9, 12
Shunt VAR compensators	9	Buses: 10, 12, 15, 17, 20, 21, 23, 24, 29	3	Buses: 18, 25, 53
Transformers with tap changing	4	Branches: 11, 12, 15, 36	17	Branches: 19, 20, 31, 35, 36, 37, 41, 46, 54, 58, 59, 65, 66, 71, 73, 76, 80
Control variables	24	-	33	-

TABLE 2. Different case studies of the MOOPF problem in this study.

Scenarios	Fuel cost	Emissions	Active power loss	System
Case 1	✓	✓		IEEE 30-bus system
Case 2	✓		✓	
Case 3	✓	✓	✓	
Case 4	✓	✓		IEEE 57-bus system
Case 5	✓		✓	
Case 6	✓	✓	✓	

Step 9: Family (\mathbf{F}_i) is created for each member of the search group based on Eq. (20).

Step 10: Save new created solutions in an advanced archive. Integrate the current archive and advanced archive.

Step 11: New Pareto archive is defined by selecting the best N_Ω solution from the combined archive.

Step 12: Perform selection of the new search group as follows:

- Global phase: Create a search group \mathbf{R}^{k+1} by selecting the best member of each family.
- Local phase: Create a search group \mathbf{R}^{k+1} by selecting n_g best solutions from the archive.

Step 13: Define α^{k+1} as in Eq. (21).

Step 14: If $i \geq Iter_{max}$, go to Step 15; otherwise, return to Step 7.

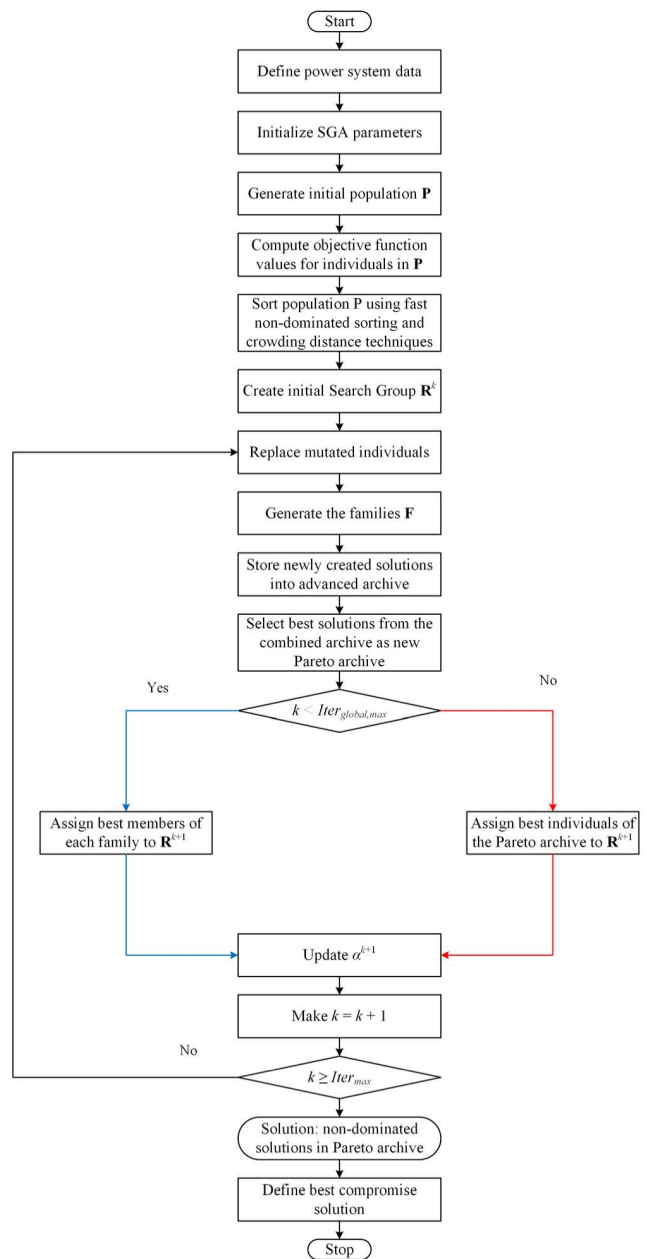
Step 15: Solutions are yielded: nondominated solutions in the final archive.

Step 16: Determine the best compromise solution as in Section III.E.3.

Fig. 5 depicts the flowchart of MOSGA for solving the MOOPF problem.

IV. SIMULATION RESULTS

The applicability of MOSGA in solving the MOOPF problem was analyzed and verified using IEEE 30- and 57-bus systems, which are detailed in Table 1. Furthermore, six distinct case studies were used, as listed in Table 2, where the objective functions are ticked in the respective boxes for a particular case study. The simulation calculations were performed using MATLAB 2019b. The parameter settings of

**FIGURE 5.** Flow chart of MOSGA for solving the MOOPF problem.

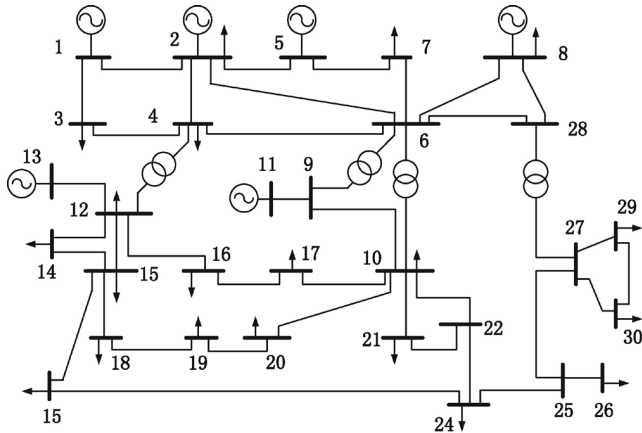
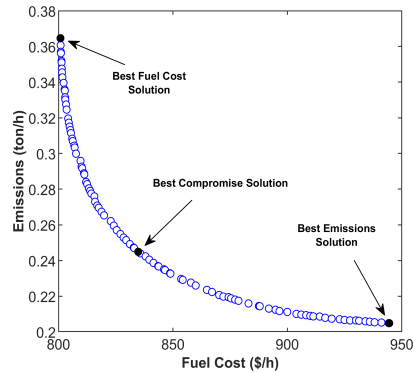
MOSGA were set as follows: $n_{pop} = 100$, $n_g = 20$, $n_{mut} = 5$, $\alpha = 2$, $N_\Omega = 100$, and $Iter_{global,max} = 0.3Iter_{max}$. Furthermore, the maximum iterations ($Iter_{max}$) were set at 300 for the 30-bus system and 500 for the 57-bus system. The MOSGA executed 30 independent trials for each case, and the optimal results were analyzed.

A. IEEE 30-BUS SYSTEM

First, the MOSGA was assessed using a 30-bus system. Fig. 6 illustrates the topology diagram of this system; detailed data can be found in [48]. The constants for fuel cost and emissions are provided in Table 3. For the initial case, the fuel

TABLE 3. IEEE 30-bus system: fuel cost and emissions constants [1], [48].

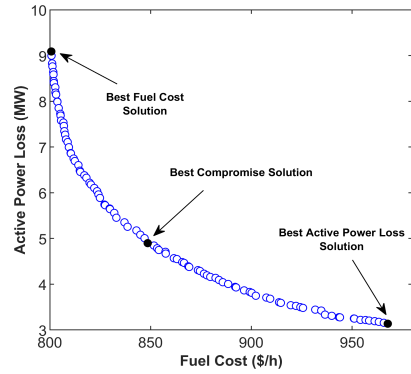
Generator	a	b	c	α	β	γ	ω	μ
G ₁	0	2	0.00375	0.04091	-0.05554	0.0649	0.0002	2.857
G ₂	0	1.75	0.0175	0.02543	-0.06047	0.05638	0.0005	3.333
G ₅	0	1	0.0625	0.04258	-0.05094	0.04586	0.000001	8
G ₈	0	3.25	0.00834	0.05326	-0.0355	0.0338	0.002	2
G ₁₁	0	3	0.025	0.04258	-0.05094	0.04586	0.000001	8
G ₁₃	0	3	0.025	0.06131	-0.05555	0.05151	0.00001	6.667

**FIGURE 6.** IEEE 30-bus test system.**FIGURE 7.** Pareto optimal front for Case 1.

cost was \$901.85/h, emissions were 0.2391 ton/h, and active power loss was 5.7866 MW.

1) CASE 1

In Case 1, the MOSGA was used to optimize the fuel cost and emissions concurrently. Fig. 7 depicts the tradeoff curve relationship between the fuel cost and emissions in the Pareto optimal front obtained by the MOSGA. It can be observed that MOSGA has a Pareto optimal front with a highly uniform distribution. Table 4 summarizes the permissible limits of the control variables and the results for the best compromise solution and best solutions for the individual objectives (corresponding to the outer extremes of the Pareto front) for Case 1. Table 4 also lists the data for the initial case of the 30-bus system. The fuel cost for the initial case was

**FIGURE 8.** Pareto optimal front for Case 2.

\$901.85/h, and the emissions amounted to 0.2391 ton/h. For the simultaneous optimization of cost and emissions, the optimal results of the best compromise solution achieved by the MOSGA were \$830.6940/h and 0.2495 ton/h, respectively. Based on the results, the reduction in fuel cost associated with the best compromise solution was 7.8902%; however, emissions increased slightly by 4.3679% compared to the initial case.

Table 5 presents a comparative analysis of the best individual solutions (i.e., the solutions with the lowest fuel cost and lowest emissions) for Case 1. Most previous studies have only reported the best compromise solutions without reporting the best individual results. Table 5 shows that the MOSGA was able to obtain the best individual solutions for both fuel cost and active power loss objectives. Further, the MOSGA obtained a vast range for the individual objectives, thus demonstrating that MOSGA provided a diverse Pareto optimal front in this case. Table 6 compares the best compromise solution from MOSGA with those of other optimization algorithms. It can be seen that the MOSGA solution (fuel cost of \$830.69/h and emissions of 0.2495 ton/h) dominated the ESDE [22] (fuel cost of \$833.47/h and emissions of 0.2540 ton/h) and ESDE-EC [22] (fuel cost of \$831.09/h and emissions of 0.2510 ton/h). Moreover, the solution provided by MOSGA was not inferior to those provided by the other algorithms in Table 6. Hence, MOSGA has great potential and advantages for finding a highly competitive solution.

2) CASE 2

In Case 2, the fuel cost and active power loss objective functions were investigated. These objective functions were

TABLE 4. Simulation results for Cases 1 and 2.

Parameters	Min	Max	Initial case	Case 1			Case 2		
				Best fuel cost solution	Best emissions solution	Best compromise solution	Best fuel cost solution	Best active power loss solution	Best compromise solution
P _{G2} (MW)	20	80	80	48.8384	67.7663	57.7838	48.4680	79.9976	53.7885
P _{G5} (MW)	15	50	50	21.5761	50	27.9181	21.3721	50	35.4674
P _{G8} (MW)	10	35	20	21.5033	35	34.9750	21.3717	34.9748	34.8833
P _{G11} (MW)	10	30	20	12.1621	30	26.9658	11.9324	30	29.2219
P _{G13} (MW)	12	40	20	12.0006	40	22.8432	12.0000	40	25.9343
V _{G1} (pu)	0.95	1.1	1.05	1.0802	1.0426	1.0723	1.0863	1.0647	1.0688
V _{G2} (pu)	0.95	1.10	1.04	1.0611	1.0365	1.0545	1.0665	1.0602	1.0581
V _{G5} (pu)	0.95	1.10	1.01	1.0335	1.0153	1.0330	1.0330	1.0414	1.0360
V _{G8} (pu)	0.95	1.10	1.01	1.0365	1.0280	1.0352	1.0402	1.0486	1.0460
V _{G11} (pu)	0.95	1.10	1.05	1.0998	1.0989	1.0819	1.0592	1.0986	1.0789
V _{G13} (pu)	0.95	1.10	1.05	1.0475	1.0617	1.0666	1.0282	1.0394	1.0369
Q _{C10} (MVar)	0	5	0	1.6266	0.3442	1.5416	4.1166	0.8715	2.7526
Q _{C12} (MVar)	0	5	0	0.5875	4.2663	2.3732	0.4776	2.0860	1.5039
Q _{C15} (MVar)	0	5	0	0.0531	0.2863	0.2588	4.2927	0.6747	2.3835
Q _{C17} (MVar)	0	5	0	3.4814	3.3376	4.0750	2.6026	4.5001	3.8742
Q _{C20} (MVar)	0	5	0	4.4918	3.6352	3.5656	2.4360	3.0776	3.3019
Q _{C21} (MVar)	0	5	0	4.6638	4.0977	4.5572	3.2793	4.8179	4.3659
Q _{C23} (MVar)	0	5	0	3.6489	1.4241	3.9293	0.5889	0.4680	2.1398
Q _{C24} (MVar)	0	5	0	4.3316	4.9897	4.3697	4.5454	4.5467	4.1373
Q _{C29} (MVar)	0	5	0	1.6863	2.7063	2.3419	4.8847	1.8568	0.9911
T ₁₁ (pu)	0.90	1.10	1.078	1.0634	0.9733	0.9879	1.0421	1.0335	1.0125
T ₁₂ (pu)	0.90	1.10	1.069	0.9798	1.0872	1.0893	0.9104	0.9721	0.9744
T ₁₅ (pu)	0.90	1.10	1.032	0.9828	1.0574	0.9874	0.9697	0.9629	0.9869
T ₃₆ (pu)	0.90	1.10	1.068	0.9799	0.9812	0.9901	0.9991	0.9784	0.9967
Fuel Cost (\$/h)	-	-	901.8515	800.6248	945.1585	830.6940	800.7040	967.7068	848.5596
Emission (ton/h)	-	-	0.2391	0.3639	0.2048	0.2495	0.3668	0.2073	0.2356
Real Power Loss (MW)	-	-	5.7866	8.9987	3.4172	5.6995	9.0888	3.1360	4.8975
P _{G1} (MW)	50	200	99.1866	176.3182	64.0509	118.6137	177.3445	51.5636	109.0020
Q _{G1} (MVar)	-20	200	-1.3109	0.9443	-9.6872	9.1089	6.0652	-2.4300	-4.6989
Q _{G2} (MVar)	-20	100	15.2817	13.4541	-0.7099	-2.2592	23.7329	8.3352	11.3121
Q _{G5} (MVar)	-15	80	16.3900	27.2022	17.2722	29.1253	24.8678	22.3699	24.8913
Q _{G8} (MVar)	-15	60	13.3507	21.3290	23.5492	18.3755	36.6464	32.1425	35.4773
Q _{G11} (MVar)	-10	50	37.9278	34.8984	27.6444	19.1973	14.5086	27.7963	18.3381
Q _{G13} (MVar)	-15	60	39.6254	6.1208	28.8704	14.6745	-5.3058	-4.4532	0.3697

TABLE 5. Comparative analysis of best individual solutions for Case 1.

Methods	Best fuel cost solution		Best emissions solution	
	Fuel cost (\$/h)	Emissions (ton/h)	Fuel cost (\$/h)	Emissions (ton/h)
MOSGA	800.6248	0.3639	945.1585	0.2048
MSFLA [14]	802.287	0.3723	951.5106	0.2056
MTLBO [16]	801.8925	0.3665	945.1965	0.20493
GBICA [21]	801.1513	0.3296	944.6516	0.2049
MGBICA [21]	801.1409	0.3296	942.8401	0.2048

simultaneously minimized using MOSGA. Fig. 8 shows a graphical representation of the evenly distributed Pareto optimal front yielded from MOSGA. Table 4 lists the optimal results for the control variables and objective functions for the fuel cost solution, active power loss solution, and the best compromise solution for Case 2. The initial case had a fuel cost of \$901.85/h and an active power loss of 5.7866 MW. The optimal results obtained by MOSGA were a fuel cost of \$848.56/h and an active power loss of 4.8975 MW, which were 5.9092% and 15.3642%, respectively, which were lower than the initial case. It is apparent that the fuel cost and active power loss were both significantly reduced using MOSGA.

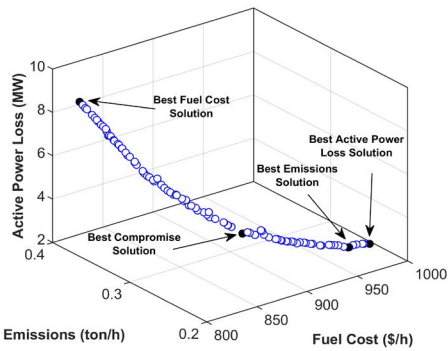
TABLE 6. Comparison of best compromise solutions for Case 1.

Methods	Fuel cost (\$/h)	Emissions (ton/h)
MOSGA	830.6940	0.2495
MSFLA [14]	823.278	0.29078
GBICA [21]	830.8524	0.2488
MGBICA [21]	830.8514	0.2484
ESDE [22]	833.474	0.2540
ESDE-EC [22]	831.0943	0.2510
ESDE-MC [22]	830.718	0.2483
ISPEA [23]	865.9499	0.2234
SPEA2 [23]	860.9832	0.2305
NSGA-II [23]	850.9166	0.2442
rNSGA-II [23]	848.1499	0.2464
MOEA/D-SF [29]	829.515	0.2501
MPIO-PFM [30]	833.1703	0.2397
MPIO-COSR [30]	832.4655	0.2351
MOPSO [31]	835.3988	0.2386
NMBAS [31]	831.4393	0.2337
MHBAS [37]	832.0355	0.2337
MDE [37]	833.1728	0.2346
IMOMRFO [38]	817.9615	0.2736

Table 7 compares the best compromise solution obtained by MOSGA with the reported results for the other methods for Case 2. Although the best compromise solution of

TABLE 7. Comparison of best compromise solutions for Case 2.

Methods	Fuel cost (\$/h)	Active power loss (MW)
MOSGA	848.5596	4.8975
ESDE [22]	828.8413	5.5901
ESDE-EC [22]	827.9487	5.4524
ESDE-MC [22]	827.1592	5.2270
MPIO-PFM [30]	832.2274	5.1270
MPIO-COSR [30]	831.5576	5.1085
MOPSO [31]	837.3469	5.2635
NMBAS [31]	831.1550	5.0707
DE-PFA [33]	833.4465	5.1354
NSGA-II [33]	835.4439	5.1599
HFBA-COFS [33]	832.3203	5.0796
MHBAS [37]	832.1236	5.0566
MDE [37]	833.7892	5.1517

**FIGURE 9.** Pareto optimal front for Case 3.

MOSGA (fuel cost of \$848.56/h and active power loss of 4.8975 MW) was not substantially better than those in the literature, MOSGA obtained the lowest active power loss value in its best compromise solution. Thus, the proposed MOSGA performed better than other methods in producing a compromise solution.

3) CASE 3

MOSGA was employed for the case with three optimized objective functions to verify its performance in detail. In this case, the fuel cost, emissions, and active power loss are optimized concurrently. Fig. 9 shows the Pareto optimal solutions generated by MOSGA, which shows the relationships between the three objectives. These solutions cover the entire Pareto optimal front with a uniform distribution. From Fig. 9, it can be observed that the three objectives are contradictory. Table 8 presents the results for the best fuel cost, emissions, active power loss solutions, and the best compromise solution acquired by MOSGA. The best compromise solution was obtained from the Pareto optimal set to offer an operating point for solving the MOOPF problem with a fuel cost of \$857.58/h, emissions of 0.2288 ton/h, and an active power loss of 4.7379 MW, representing reductions of 4.9089%, 4.2911%, and 18.1223%, respectively, compared to the initial case.

A comparison of the optimal compromise solutions for Case 3 is presented in Table 9. In an optimization problem

TABLE 8. Simulation results for Case 3.

Parameters	Best fuel cost solution	Best emission solution	Best power loss solution	Best compromise solution
P_{G2} (MW)	48.8333	67.5383	80	62.7678
P_{G5} (MW)	21.3432	50	49.9984	35.8914
P_{G8} (MW)	22.7468	35	35	33.9785
P_{G11} (MW)	10.6058	30	30	27.0821
P_{G13} (MW)	12.0000	40	40	28.2992
V_{G1} (pu)	1.0794	1.0601	1.0627	1.0665
V_{G2} (pu)	1.0592	1.0546	1.0583	1.0591
V_{G5} (pu)	1.0258	1.0316	1.0414	1.0331
V_{G8} (pu)	1.0333	1.0357	1.0467	1.0389
V_{G11} (pu)	1.0358	1.0920	1.0830	1.0640
V_{G13} (pu)	1.0759	1.0353	1.0481	1.0479
Q_{C10} (MVar)	2.3018	3.3442	2.3114	2.9297
Q_{C12} (MVar)	1.5279	1.9026	2.3894	2.1273
Q_{C15} (MVar)	4.2124	4.0036	4.2098	3.8724
Q_{C17} (MVar)	3.4056	4.0752	4.1296	4.0215
Q_{C20} (MVar)	3.9761	1.5920	1.2701	2.6057
Q_{C21} (MVar)	2.3341	4.4307	4.9947	3.6991
Q_{C23} (MVar)	3.2480	0.6424	1.5073	2.2949
Q_{C24} (MVar)	2.9667	3.6876	4.3224	3.7854
Q_{C29} (MVar)	1.3885	1.7465	2.2164	1.7030
T_{11} (pu)	0.9961	1.0992	1.0990	1.0577
T_{12} (pu)	0.9461	0.9162	0.9013	0.9406
T_{15} (pu)	1.0275	0.9777	0.9730	0.9935
T_{36} (pu)	0.9588	0.9729	0.9861	0.9843
Fuel Cost (\$/h)	800.8485	944.5370	967.6848	857.5806
Emission (ton/h)	0.3661	0.2048	0.2073	0.2288
Real Power Loss (MW)	9.0956	3.3171	3.1125	4.7379
P_{G1} (MW)	176.9665	64.1788	51.5141	100.1188
Q_{G1} (MVar)	2.3604	-3.8258	-4.1279	-9.0728
Q_{G2} (MVar)	16.3007	15.1535	5.6822	20.0033
Q_{G5} (MVar)	24.3121	19.7086	23.7524	22.9222
Q_{G8} (MVar)	33.5186	20.0897	28.5547	24.6227
Q_{G11} (MVar)	0.4452	36.8513	29.7905	20.2039
Q_{G13} (MVar)	24.0828	-0.5312	-0.2114	6.5611

TABLE 9. Comparison of best compromise solutions for Case 3.

Methods	Fuel cost (\$/h)	Emissions (ton/h)	Active power loss (MW)
MOSGA	857.5806	0.2288	4.7379
MOEA/D-SF [29]	881.012	0.2164	4.1441
MPIO-PFM [30]	866.0601	0.2160	4.4474
MPIO-COSR [30]	863.9503	0.2126	4.3177
MOPSO [31]	868.0536	0.2168	4.4576
NMBAS [31]	863.8246	0.2123	4.2089
DE-PFA [33]	869.9216	0.2087	4.2429
NSGA-II [33]	867.9027	0.2111	5.0865
HFBA-COFS [33]	867.4262	0.2100	4.1544
FAHSPSO-DE [34]	867.9808	0.2666	5.5638
MHBAS [37]	864.4699	0.2114	4.2476
MDE [37]	867.1991	0.2116	4.7428

with three objective functions, as in Case 3, no single solution can outperform the others for all three objective functions. However, MOSGA obtained a better fuel cost value in the best compromise solution than the others in Case 3. Therefore, MOSGA achieved the most advantageous solution for Case 3.

As can be seen from the results obtained for Case 3, the implementation of MOSGA to solve the MOOPF problem led to a substantial enhancement in all three objective functions.

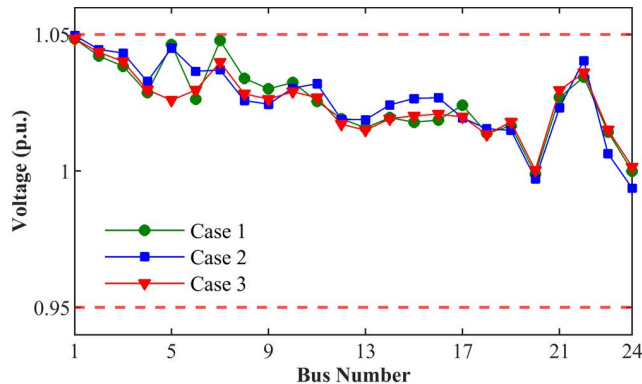


FIGURE 10. Voltage magnitude at load buses for best compromise solution for Cases 1, 2, and 3.

Therefore, the best compromise solution fulfilled all objective functions concurrently to a great extent. Furthermore, one of the crucial aspects of the MOOPF problem is maintaining the dependent variables within specific ranges. Tables 4 and 9 also show the values of the dependent variables for Cases 1, 2, and 3, including the active power generation at the slack bus and the reactive power outputs of the generators. Moreover, Fig. 10 shows the voltages at the load buses of the system for Cases 1, 2, and 3. It is worth noting that this study applied voltage limits at the load buses of 0.95 p.u.–1.05 p.u. for the IEEE 30-bus system, as referenced in [29], which is a much narrower range than the range of 0.90 p.u.–1.10 p.u. used in most other studies. A narrower range increases the difficulty of solving the MOOPF problem in case studies. It is evident from Table 4, Table 9, and Fig. 10 that all boundaries were satisfied for the constraining variables. Therefore, the superiority of the proposed MOSGA was proven in terms of solution feasibility and optimality, showing its overall potential and efficacy.

B. IEEE 57-BUS SYSTEM

The scalability of MOSGA was verified for application in an IEEE 57-bus system. Fig. 11 illustrates a topology diagram for the system, and the fuel cost and emission constants are listed in Table 10. The detailed data can be found in the literature [49], [50]. The system had a fuel cost of \$51348.22/h, emissions of 2.7590 ton/h, and an active power loss of 27.8637 MW for the initial case.

1) CASE 4

In this case, the performance of the MOSGA for the simultaneous optimization of the fuel cost and emissions was considered. Fig. 12 shows a graphical representation of the Pareto optimal front generated by MOSGA, demonstrating a trade-off curve of the fuel cost and emissions objectives. Similar to the 30-bus system, MOSGA acquired a uniformly distributed Pareto optimal front. Table 11 lists the permissible limits of the control variables and the simulation results for Case 4. The fuel cost and emissions were significantly

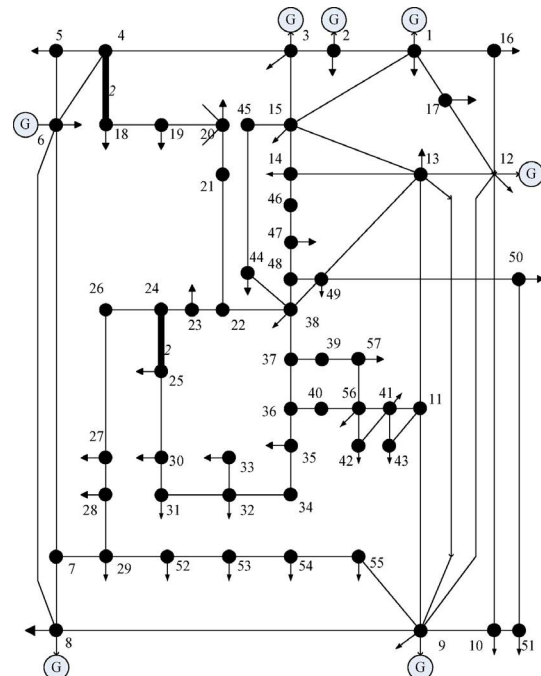


FIGURE 11. IEEE 57-bus system.

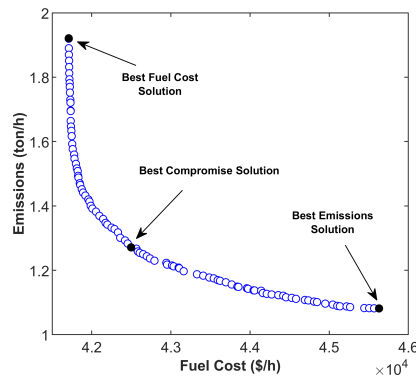


FIGURE 12. Pareto optimal front for Case 4.

reduced from \$51319.83/h and 2.7574 ton/h in the initial case to 42497.0130 \$/h and 1.2712 ton/h, yielding reductions of 17.1918% and 53.8992%, respectively.

Table 12 presents the best individual objectives obtained by the MOSGA with the available tabulated results of GBICA and MGBICA for Case 4. Because MOSGA can achieve a minimum fuel cost of \$41709.15/h and minimum emissions of 1.0814 ton/h, MOSGA outperformed GBICA [21] and MGBICA [21] on individual best objectives. Thus, the Pareto optimal front of MOSGA has better diversity characteristics than those of GBICA [21] and MGBICA [21]. A comparison of the best compromise solution acquired by MOSGA with studies available in the literature is presented in Table 13. Based on the fuel cost and emissions values, the best compromise solution of MOSGA (\$42497.01/h and 1.2712 ton/h) was better than the solutions offered by nondominated sorting genetic algorithm (NSGA-II) [23], rNSGA-II [23], and

TABLE 10. IEEE 57-bus system: fuel cost and emissions constants [12], [29].

Generator	a	b	c	α	β	γ	ω	μ
G ₁	0	20	0.0775795	0.04	-0.05	0.06	0.00002	0.5
G ₂	0	40	0.01	0.03	-0.06	0.05	0.00005	1.5
G ₃	0	20	0.25	0.04	-0.05	0.04	0.00001	1
G ₆	0	40	0.01	0.035	-0.03	0.035	0.00002	0.5
G ₈	0	20	0.0222222	0.05	-0.05	0.045	0.00004	2
G ₉	0	40	0.01	0.045	-0.04	0.05	0.00001	2
G ₁₂	0	20	0.0322581	0.06	-0.05	0.05	0.00001	1.5

TABLE 11. Simulation results for Cases 4 and 5.

Parameters	Min	Max	Initial case	Case 4			Case 5		
				Best fuel cost solution	Best emissions solution	Best compromise solution	Best fuel cost solution	Best active power loss solution	Best compromise solution
P _{G2} (MW)	0	100	0	94.7288	100	99.0854	62.1902	48.3060	50.1557
P _{G3} (MW)	0	140	40	46.5434	140	78.0144	45.5310	76.1346	53.8275
P _{G6} (MW)	0	100	0	76.0927	100	99.1364	83.2251	99.3525	94.3328
P _{G8} (MW)	0	550	450	460.4895	293.7082	358.8915	466.5181	335.2876	388.6894
P _{G9} (MW)	0	100	0	85.1985	100	96.9095	99.9767	98.6388	
P _{G12} (MW)	0	410	310	360.8083	299.1884	337.5615	366.0819	410	408.9298
V _{G1} (pu)	0.95	1.10	1.01	1.0523	1.0541	1.0474	1.0377	1.0558	1.0522
V _{G2} (pu)	0.95	1.10	1.01	1.0496	1.0522	1.0465	1.0356	1.0512	1.0459
V _{G3} (pu)	0.95	1.10	1.01	1.0401	1.0575	1.0450	1.0365	1.0470	1.0430
V _{G6} (pu)	0.95	1.10	1.01	1.0423	1.0507	1.0459	1.0568	1.0548	1.0565
V _{G8} (pu)	0.95	1.10	1.01	1.0580	1.0451	1.0494	1.0779	1.0686	1.0692
V _{G9} (pu)	0.95	1.10	1.01	1.0314	1.0267	1.0271	1.0431	1.0446	1.0429
V _{G12} (pu)	0.95	1.10	1.01	1.0319	1.0373	1.0292	1.0334	1.0461	1.0439
Q _{C18} (MVar)	0	20	10	7.4222	7.0630	9.0291	8.5174	13.3361	10.9759
Q _{C25} (MVar)	0	20	5.9	11.9176	13.2550	13.1636	9.6620	7.6312	9.1238
Q _{C53} (MVar)	0	20	6.3	11.1146	16.1980	12.4463	11.6679	11.2120	11.4296
T ₁₉ (pu)	0.90	1.10	0.970	1.0308	1.0474	1.0435	0.9998	0.9909	0.9866
T ₂₀ (pu)	0.90	1.10	0.978	0.9490	0.9497	0.9541	0.9937	0.9924	0.9952
T ₃₁ (pu)	0.90	1.10	1.043	1.0410	1.0178	1.0384	1.0404	1.0281	1.0443
T ₃₅ (pu)	0.90	1.10	1	1.0070	0.9678	0.9743	0.9408	0.9882	0.9776
T ₃₆ (pu)	0.90	1.10	1	0.9663	0.9523	0.9619	0.9776	0.9731	0.9723
T ₃₇ (pu)	0.90	1.10	1.043	1.0493	1.0347	1.0368	1.0130	1.0160	1.0131
T ₄₁ (pu)	0.90	1.10	0.967	1.0044	1.0237	1.0180	1.0002	0.9890	0.9968
T ₄₆ (pu)	0.90	1.10	0.975	0.9688	0.9886	0.9756	0.9899	0.9887	0.9914
T ₅₄ (pu)	0.90	1.10	0.955	0.9716	0.9760	0.9741	0.9552	0.9778	0.9659
T ₅₈ (pu)	0.90	1.10	0.955	0.9808	0.9971	0.9960	0.9800	0.9773	0.9751
T ₅₉ (pu)	0.90	1.10	0.9	0.9696	0.9629	0.9705	0.9808	0.9594	0.9686
T ₆₅ (pu)	0.90	1.10	0.93	1.0069	1.0177	1.0098	0.9987	0.9845	0.9943
T ₆₆ (pu)	0.90	1.10	0.895	0.9654	0.9738	0.9674	0.9509	0.9371	0.9427
T ₇₁ (pu)	0.90	1.10	0.958	0.9575	0.9750	0.9630	0.9988	0.9603	0.9663
T ₇₃ (pu)	0.90	1.10	0.958	0.9130	0.9376	0.9344	0.9630	0.9870	0.9825
T ₇₆ (pu)	0.90	1.10	0.98	0.9942	0.9950	0.9928	1.0043	0.9865	0.9930
T ₈₀ (pu)	0.90	1.10	0.94	1.0020	1.0171	1.0209	1.0096	1.0027	0.9974
Fuel Cost (\$/h)	-	-	51319.8381	41709.1504	45629.6834	42497.0130	41708.4121	42648.8817	41994.6175
Emissions (ton/h)	-	-	2.7574	1.9209	1.0814	1.2712	2.0168	1.4199	1.5818
Active Power Loss (MW)	-	-	27.5627	15.8628	16.7935	14.3479	15.6434	10.7243	11.8514
P _{G1} (MW)	0	576	478.3627	142.8016	234.6969	192.4587	145.9877	192.4669	168.0776
Q _{G1} (MVar)	-140	200	-38.8305	56.5788	33.3677	35.0268	26.0660	36.0620	45.4098
Q _{G2} (MVar)	-17	50	79.4826	49.4320	32.6709	45.4262	49.1841	49.2801	41.2121
Q _{G3} (MVar)	-10	60	58.9447	39.3061	56.8971	48.9024	34.6511	20.9410	26.5042
Q _{G6} (MVar)	-8	25	32.7105	-7.3522	8.6278	1.4893	-1.5668	-6.8955	-1.1246
Q _{G8} (MVar)	-140	200	-16.7016	56.0622	32.9899	43.9257	80.2785	65.2478	60.0400
Q _{G9} (MVar)	-3	9	102.8637	8.7474	0.4325	8.0179	8.6811	8.7250	6.9437
Q _{G12} (MVar)	-150	155	98.8572	48.6994	81.0981	57.8460	53.4200	50.9499	51.6418

MOQRJFS [35] in previous studies, although it was not superior to the other methods. However, no method offered a significantly better solution than MOSGA's best compromise solution.

2) CASE 5

Case 5 addresses the fuel cost and active power loss, which are two conflicting objective functions. Fig. 13 shows the Pareto optimal front generated by MOSGA. Table 11 presents

TABLE 12. Comparative analysis of best individual solutions for Case 4.

Methods	Best fuel cost solution		Best emissions solution	
	Fuel cost (\$/h)	Emissions (ton/h)	Fuel cost (\$/h)	Emissions (ton/h)
MOSGA	41709.1504	1.9209	45629.6834	1.0814
MSFLA [14]	41740.2884	1.8683	43541.0221	1.1881
MTLBO [16]	41715.7101	1.8445	43641.4250	1.1724

TABLE 13. Comparison of best compromise solutions for Case 4.

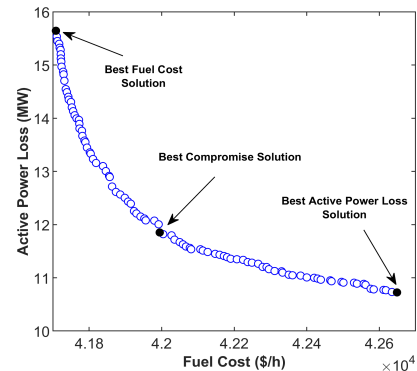
Methods	Fuel cost (\$/h)	Emissions (ton/h)
MOSGA	42497.0130	1.2712
GBICA [21]	42138.3695	1.3941
MGBICA [21]	42369.0664	1.2940
ESDE [22]	42863.3243	1.2662
ESDE-EC [22]	42863.2116	1.2387
ESDE-MC [22]	42857.4869	1.2191
ISPEA [23]	42444.5535	1.2904
SPEA2 [23]	42320.2545	1.4054
NSGA-II [23]	43567.7653	1.2979
rNSGA-II [23]	42635.7170	1.3784
MPIO-PFM [30]	43205.8477	1.2386
MPIO-COSR [30]	43131.2743	1.2314
MOPSO [31]	43279.6398	1.2546
NMBAS [31]	43117.8602	1.2245
DE-PFA [33]	43331.7568	1.2180
NSGA-II [33]	43353.5661	1.2272
HFBA-COFS [33]	43259.3013	1.2129
MOJFS [35]	43888.2320	1.2383
MOQRJFS [35]	43713.0146	1.3074
IHOA [36]	43864.8798	1.2192
MHBAS [37]	43174.05	1.2211
MDE [37]	43505.90	1.2236
IMOMRFO [38]	41742.9442	1.7912

TABLE 14. Comparison of best compromise solutions for Case 5.

Methods	Fuel cost (\$/h)	Active power loss (MW)
MOSGA	41994.6175	11.8514
ESDE [22]	42020.7439	12.2155
ESDE-EC [22]	42013.3395	11.9668
ESDE-MC [22]	41998.3588	11.8415
NSGA-II [33]	42125.6042	11.1296
HFBA-COFS [33]	42122.0140	10.6995
MOJFS [35]	42591.8712	15.1461
MOQRJFS [35]	41846.2247	15.8873
IHOA [36]	42419.5253	10.8192
MHBAS [37]	42084.81	10.5043
MDE [37]	42125.83	10.9193

the simulation results for case 5. The fuel cost and active power loss for the best compromise solution were \$41994.61/h and 11.8514 MW, respectively. Compared with the initial case (\$51319.83/h and 27.5627 MW), the fuel cost and active power loss were considerably reduced by 18.1708% and 57.0020%, respectively.

A comparative study of compromise solutions for Case 5 is presented in Table 14. MOSGA found a good-quality solution, with a fuel cost of \$41994.61/h and an active power loss of 11.8514 MW. The proposed MOSGA not only produced better results than ESDE [22], ESDE-EC [22], and MOJFS [35] but also yielded the second-best value for the fuel cost objective. Therefore, MOSGA has an advantage

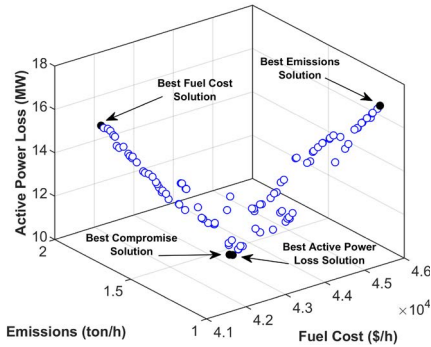
**FIGURE 13.** Pareto optimal front for Case 5.**TABLE 15.** Simulation results for Case 6.

Parameters	Best fuel cost solution	Best emission solution	Best power loss solution	Best compromise solution
P _{G2} (MW)	78.5012	100	85.8691	86.4438
P _{G3} (MW)	44.5938	140	89.8390	89.5379
P _{G6} (MW)	90.0785	100	98.9214	99.1791
P _{G8} (MW)	455.7015	293.2647	315.4463	320.1753
P _{G9} (MW)	92.4330	100	99.8371	99.7626
P _{G12} (MW)	362.5118	296.4172	410	410
V _{G1} (pu)	1.0530	1.0736	1.0664	1.0661
V _{G2} (pu)	1.0494	1.0686	1.0647	1.0640
V _{G3} (pu)	1.0414	1.0520	1.0601	1.0604
V _{G6} (pu)	1.0560	1.0463	1.0596	1.0590
V _{G8} (pu)	1.0733	1.0512	1.0623	1.0624
V _{G9} (pu)	1.0443	1.0322	1.0462	1.0460
V _{G12} (pu)	1.0396	1.0374	1.0557	1.0550
Q _{C18} (MVar)	13.2135	14.2586	7.9398	7.9178
Q _{C25} (MVar)	14.5220	9.3637	13.5850	13.6242
Q _{C53} (MVar)	16.5320	5.9090	12.7079	12.8168
T ₁₉ (pu)	0.9683	1.0091	0.9819	0.9821
T ₂₀ (pu)	1.0077	1.0073	1.0202	1.0214
T ₃₁ (pu)	1.0070	1.0392	1.0264	1.0277
T ₃₅ (pu)	1.0423	1.0361	1.0631	1.0631
T ₃₆ (pu)	0.9997	0.9622	1.0007	1.0011
T ₃₇ (pu)	1.0484	1.0694	1.0552	1.0561
T ₄₁ (pu)	1.0022	0.9734	0.9959	0.9972
T ₄₆ (pu)	0.9383	0.9488	0.9587	0.9575
T ₅₄ (pu)	0.9570	0.9737	0.9504	0.9501
T ₅₈ (pu)	0.9870	0.9762	0.9876	0.9885
T ₅₉ (pu)	0.9671	0.9876	0.9725	0.9735
T ₆₅ (pu)	0.9651	0.9982	0.9743	0.9742
T ₆₆ (pu)	0.9567	0.9423	0.9486	0.9479
T ₇₁ (pu)	1.0093	1.0243	1.0104	1.0106
T ₇₃ (pu)	1.0119	1.0344	0.9962	0.9949
T ₇₆ (pu)	0.9722	0.9777	0.9241	0.9241
T ₈₀ (pu)	1.0316	1.0379	1.0126	1.0140
Fuel Cost (\$/h)	41693.009	45694.610	42872.921	42815.7887
Emissions (ton/h)	1.8752	1.0812	1.3157	1.3219
Active Power Loss (MW)	15.3230	16.9005	10.7416	10.7648
P _{G1} (MW)	142.3032	238.0186	161.6286	156.4660
Q _{G1} (MVar)	47.8042	76.3247	33.8950	36.9629
Q _{G2} (MVar)	49.1405	47.5704	49.9723	46.6214
Q _{G3} (MVar)	16.2189	2.7008	30.3097	33.2416
Q _{G6} (MVar)	-6.3497	2.9874	2.2801	0.4364
Q _{G8} (MVar)	63.2061	58.4527	37.8552	38.5718
Q _{G9} (MVar)	8.7337	5.1215	8.5366	8.4886
Q _{G12} (MVar)	51.9927	58.3418	57.7480	56.4276

over comparable methods for the quality of the Pareto optimal solutions obtained.

TABLE 16. Comparison of best compromise solutions for Case 6.

Methods	Fuel cost (\$/h)	Emissions (ton/h)	Active power loss (MW)
MOSGA	42815.7887	1.3219	10.7648
MPIO-PFM [30]	43133.9896	1.5027	11.7899
MPIO-COSR [30]	42133.3305	1.4360	11.7711
DE-PFA [33]	42387.1559	1.5175	11.3076
NSGA-II [33]	42887.0244	1.4572	11.6865
HFBA-COFS [33]	42856.4896	1.3436	11.6782
FAHPSO-DE [34]	44759.7757	1.6035	13.1377
MOJFS [35]	45064.711	1.1891	15.0875
MOQRJFS [35]	44315.7483	1.3597	14.2560

**FIGURE 14.** Pareto optimal front for Case 6.

3) CASE 6

In this case, MOSGA simultaneously optimizes three objective functions: fuel cost, emissions, and active power loss. The Pareto optimal front generated by MOSGA is depicted in Fig. 14. The simulation results for Case 6 are summarized in Table 15. In the best compromise solution, the MOSGA yielded a fuel cost of \$42815.78/h, emissions of 1.3219 t/h, and an active power loss of 10.7648 MW, which represented reductions of 16.5707%, 52.0605%, and 60.9443%, respectively, in comparison to the initial case.

Table 16 compares the best compromise solution obtained by MOSGA with the results of the other methods reported in the literature for Case 6. In the tri-objective optimization of Case 6, MOSGA outperformed MPIO-PFM [30], NSGA-II [33], HFBA-COFS [33], FAHPSO-DE [34], and MOQRJFS [35] for all three objectives in the best compromise solution. No other method was superior with respect to all of the objective functions. Nevertheless, MOSGA achieved better emissions and active power loss in the best compromise solution than other methods. It can be concluded that MOSGA is noticeably superior to all the algorithms considered in generating a better Pareto optimal front.

From the results of Case 6, it may be observed that the application of MOSGA to the MOOPF problem demonstrated a significant advance in all three objectives. Moreover, Tables 11 and 15 present the results of the dependent variables corresponding to the solutions considered for Cases 4, 5, and 6, and show that all the obtained values of the dependent variables were within the allowable limits of the system.

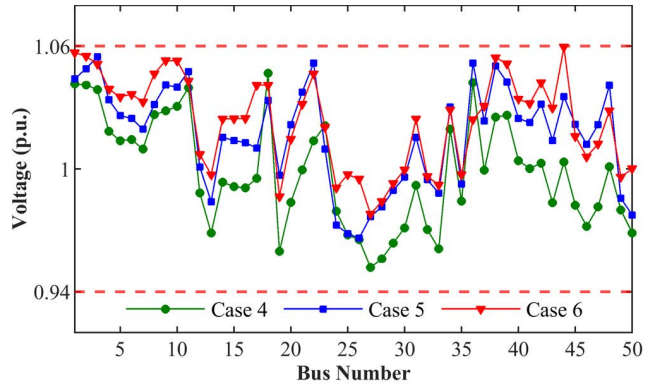
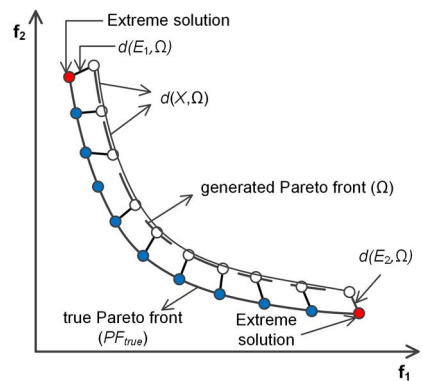
**FIGURE 15.** Voltage magnitude at load buses for best compromise solution for Cases 4, 5, and 6.**FIGURE 16.** Schematic view of the Δ metric.

Fig. 15 shows the voltages at the load buses for cases 4, 5, and 6; all the results are within the allowable voltage limits (0.94 p.u.–1.06 p.u.) of the load buses for the 57-bus system. Again, the optimization results confirm the advantages of MOSGA in terms of solution optimality and feasibility.

C. NUMERICAL COMPARISONS

To further verify the advantages of MOSGA, its performance was compared with those of three well-known algorithms: the nondominated sorting genetic algorithm II (NSGA-II) [44], multi-objective ant lion optimizer (MOALO) [51], multi-objective grasshopper optimization algorithm (MOGOA) [52], and multi-objective lichtenberg algorithm (MOLA) [53]. The control parameters for MOSGA were the same as those given in Sections V.A and V.B. With NSGA-II, the crossover probability was set to 0.9, the mutation probability to 0.5, and the mutation and crossover operators to 20. In MOGOA, the minimum and maximum values of the decreasing coefficient (c_{\min} and c_{\max}) were set to 0.00004 and 1, respectively. As for MOLA, the refinement, stick probability, creation radius, and switching factor were chosen as 0.4, 1, 150, and 0, respectively. For a fair comparison, the other main parameters were set to the same value for all algorithms: population size = 100, Pareto archive size = 100, and maximum iterations = 300 for the 30-bus

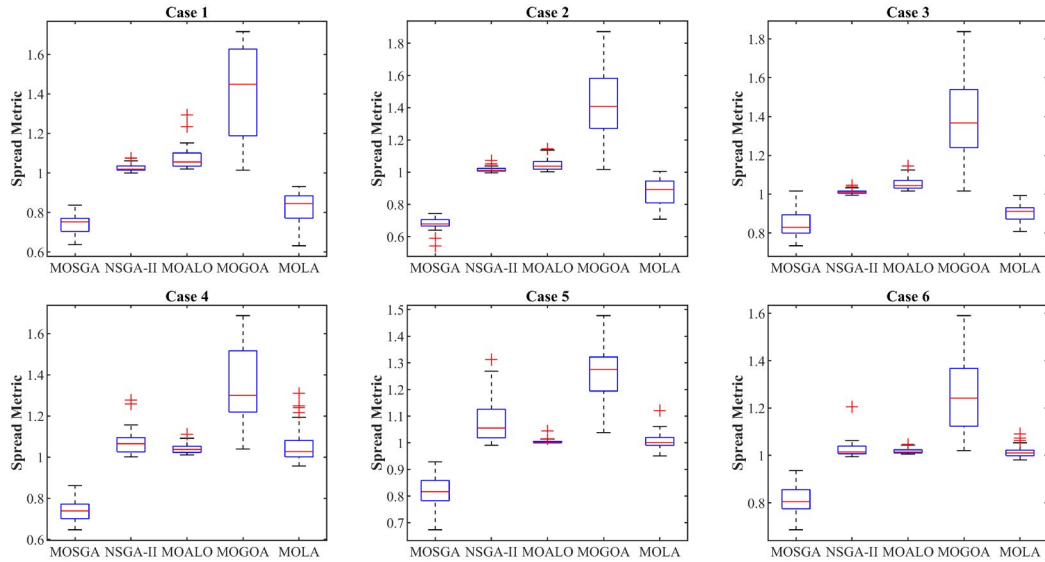


FIGURE 17. Box plots of Δ metric of multi-objective algorithms.

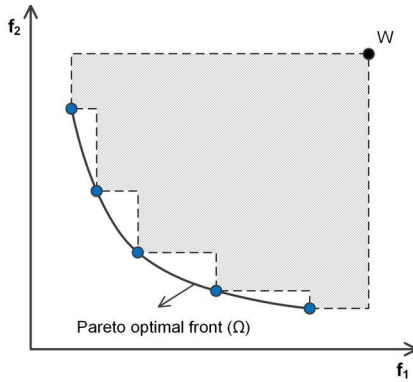


FIGURE 18. Schematic view of the HV metric.

system and 500 for the 57-bus system. In each case, the optimization outputs were examined in 30 independent trials for each algorithm based on two performance metrics: spread and hypervolume.

1) SPREAD INDICATOR

The spread (Δ) metric is used to show the diversity of the non-dominated solutions obtained by an algorithm. Fig. 16 shows a schematic view of the Δ metric, which measures the distribution of Pareto optimal solutions and the spread of extreme solutions, as shown below [54]:

$$\Delta = \frac{\sum_{i=1}^m d(E_i, \Omega) + \sum_{X \in \Omega} |d(X, \Omega) - \bar{d}|}{\sum_{i=1}^m d(E_i, \Omega) + (|\Omega| - m) \bar{d}} \quad (31)$$

where

$$d(X, \Omega) = \min_{Y \in \Omega, Y \neq X} \|F(X) - F(Y)\| \quad (32)$$

$$\bar{d} = \frac{1}{|\Omega|} \sum_{X \in \Omega} d(X, \Omega) \quad (33)$$

where Ω denotes the generated Pareto optimal front, and E_i denotes the i^{th} extreme solution in the true Pareto front. The minimum value of the Δ metric demonstrates the best diversity (better extent of distribution and spread) in a Pareto optimal set.

Table 17 compares the Δ metrics for different algorithms. It can be inferred that the performance of MOSGA was much better than that of the other techniques for most case studies. Fig. 17 further demonstrates the distributions of Δ metric values, with box plots of the Δ metric from MOSGA, NSGA-II, MOALO, MOGOA, and MOLA. MOSGA had the lowest median (as shown by the red line) and lowest value (as shown by the bottom solid line) for all case studies. Therefore, MOSGA had an advantage in terms of finding uniformly distributed nondominated solutions, and the nondominated sets found by MOSGA had better diversity than the other algorithms. Therefore, MOSGA had an advantage in terms of finding uniformly distributed nondominated solutions, and the nondominated sets found by MOSGA had better diversity than the other algorithms.

2) HYPERVOLUME INDICATOR

For a problem in which all objectives need to be minimized in the objective space, the hypervolume (HV) metric is used to calculate the volume enclosed by the members of a Pareto optimal set (Ω). With reference point W , hypercube v_i is mathematically created for each solution $i \in \Omega$, where solution i is a diagonal corner of the hypercube. A reference point is generated from a vector of the worst objective values. Subsequently, a union of all hypercubes is constructed, and the HV of this union can be determined [55]:

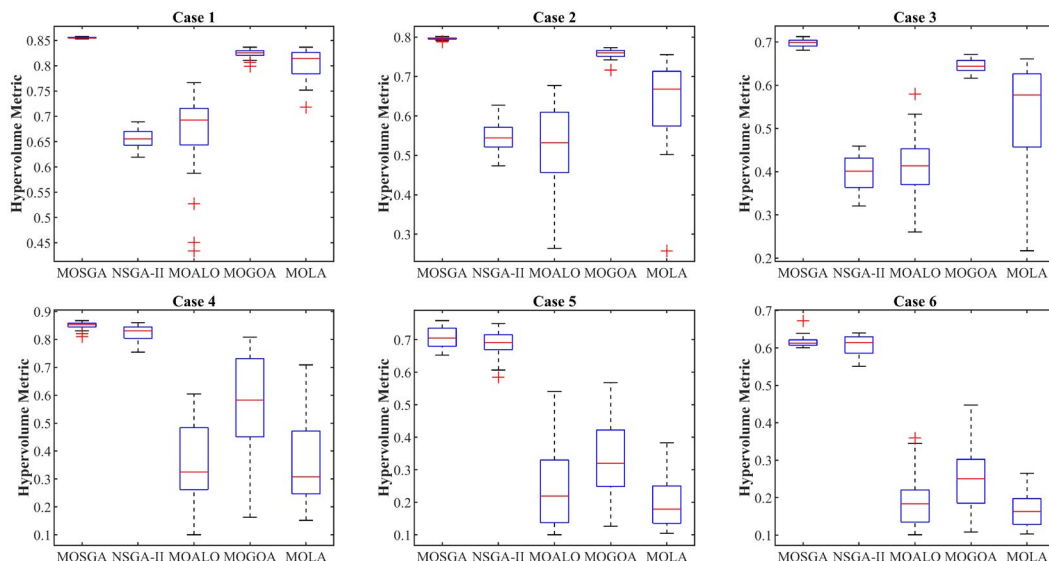
$$HV = \bigcup_{i=1}^{|\Omega|} v_i \quad (34)$$

TABLE 17. Comparative analysis of Δ indicator of multi-objective algorithms.

Case study	MOSGA		NSGA-II		MOALO		MOGOA		MOLA	
	Average	Standard deviation								
Case 1	0.7449	0.0477	1.0257	0.0206	1.0790	0.0634	1.4239	0.2165	0.8286	0.0770
Case 2	0.6800	0.0423	1.0172	0.0177	1.0495	0.0404	1.4251	0.2169	0.8733	0.0870
Case 3	0.8513	0.0663	1.0121	0.0131	1.0525	0.0319	1.3844	0.2183	0.9044	0.0500
Case 4	0.7365	0.0529	1.0753	0.0685	1.0396	0.0239	1.3401	0.1681	1.0642	0.0915
Case 5	0.8146	0.0622	1.0801	0.0809	1.0049	0.0086	1.2690	0.1092	1.0099	0.0332
Case 6	0.8105	0.0678	1.0262	0.0382	1.0187	0.0116	1.2622	0.1566	1.0152	0.0270

TABLE 18. Comparative analysis of HV indicator of multi-objective algorithms.

Case study	MOSGA		NSGA-II		MOALO		MOGOA		MOLA	
	Average	Standard deviation								
Case 1	0.8553	0.0010	0.6553	0.0190	0.6688	0.0818	0.8241	0.0082	0.8031	0.0305
Case 2	0.7958	0.0027	0.5454	0.0381	0.5206	0.1071	0.7570	0.0139	0.6381	0.1055
Case 3	0.6977	0.0087	0.3980	0.0444	0.4122	0.0756	0.6449	0.0144	0.5360	0.1174
Case 4	0.8488	0.0139	0.8226	0.0261	0.3577	0.1342	0.5685	0.1733	0.3520	0.1433
Case 5	0.7052	0.0301	0.6878	0.0372	0.2459	0.1282	0.3359	0.1199	0.1958	0.0761
Case 6	0.6172	0.0148	0.6073	0.0265	0.1940	0.0770	0.2491	0.0937	0.1669	0.0483

**FIGURE 19.** Box plots of HV metric of multi-objective algorithms.**TABLE 19.** Comparisons of computational time for multi-objective methods.

Case study	MOSGA	NSGA-II	MOALO	MOGOA	MOLA
Case 1	88.6729	246.7214	110.9443	278.9839	118.3510
Case 2	88.0776	251.5573	107.5651	280.1849	114.0078
Case 3	87.3510	241.4271	106.0865	287.3172	120.3458
Case 4	177.5833	489.8307	240.3328	645.3057	228.9240
Case 5	177.9443	488.1417	235.8115	637.5438	226.9505
Case 6	177.1172	487.9385	238.7979	650.1255	230.9661

As shown in Fig. 18, the HV is depicted as a hatched area. A method with a higher HV value is preferable.

Table 18 compares the optimal results of the different algorithms with respect to HV, which is a robust approach to evaluating an algorithm in terms of both convergence and diversity. As can be seen from Table 18, MOSGA obtained the highest HV values for all case studies. To visualize the comparative analysis of the HV metric, box plots of HV indicators from MOSGA, NSGA-II, MOALO, MOGOA, and MOLA are depicted in Fig. 19, which shows that MOSGA had the highest median and maximum values compared to the other three algorithms. Therefore, MOSGA exhibited better convergence and diversity performance than OSGA, NSGA-II, MOALO, MOGOA, and MOLA.

3) COMPUTATIONAL COST

This study used a 2.6 GHz 4-core PC with 16 GB of RAM to implement the MOSGA algorithm and four comparison methods. The computation times of these multi-objective methods are discussed in Table 19. For six case studies, MOSGA has the lowest computational cost compared to other methods, as shown in Table 19. It can be concluded that MOSGA not only obtained a better solution to the MOOPF problem but also has a very efficient computation cost.

V. CONCLUSION

In this study, the MOOPF problem was solved to address the objective functions of fuel cost, emissions, and active power loss. The new MOSGA effectively defined the optimal operation points of the control variables in power systems while meeting all operating constraints. The performance of MOSGA was demonstrated on 30- and 57-bus systems with six case studies. The implementation of MOSGA to deal with the MOOPF problem significantly reduced the fuel cost and emissions and improved the active power loss in power systems. These benefits can be clearly seen in Case 6, where the fuel cost, emissions, and active power loss levels were reduced by 16.5707%, 52.0605%, and 60.9443%, respectively, compared to the initial case. The comparison results indicate that the proposed MOSGA outperformed other techniques in terms of the quality of optimal solutions, especially for large-scale systems. MOSGA yielded well-distributed nondominated solutions that spread over the Pareto optimal front for all considered cases, which proves that MOSGA has better convergence and diversity characteristics than the other methods. Consequently, it can be concluded that MOSGA is a promising alternative for solving the MOOPF problem.

NOMENCLATURE

a_i, b_i, c_i	Cost coefficients of the i^{th} generator.
d	Crowding distance.
E	Mean operator.
$f_{(i+1),j}, f_{(i-1),j}$	j^{th} objective values for the two neighboring solutions $i + 1$ and $i - 1$ of solution i .
$f_{j,\max}, f_{j,\min}$	Largest and smallest values of the j^{th} objective function.
$F(u,x)$	Set of objective functions to be optimized.
G_{ij}, B_{ij}	Transfer conductance and susceptance between buses i and j .
$G_{q(ij)}$	Transfer conductance between buses i and j .
$g(x,u)$	Set of inequality constraints.
$h(x,u)$	Set of equality constraints.
Iter_{\max}	Maximum number of iterations.
$\text{Iter}_{\text{global},\max}$	Maximum number of iterations of the global phase.
n	Number of control variables.
NB	Number of buses.

NC	Number of shunt VAR compensators.
ND	Number of load buses.
NG	Number of generators.
n_g	Number of search group members.
NL	Number of transmission lines.
n_{mut}	Number of mutations.
n_{pop}	Population size.
n_{obj}	Number of objective functions.
n_{pf}	Number of nondominated solutions.
NT	Number of transformers.
N_{Ω}	Pareto archive size.
P_D, Q_D	Active and reactive load demands.
P_{G1}	Active power output at the slack bus.
$P_{G,i}$	Active power output of the i^{th} generator.
P_{ij}	j^{th} control variable of the i^{th} individual of population \mathbf{P} .
P_L	Active power loss in power systems.
QC	Shunt VAR compensation.
Q_G	Reactive power output of the generator.
r	Nondominated rank.
$R_{:,j}$	j^{th} column of the search group matrix.
S_L	Transmission line loadings.
t	A parameter controlling how far away a new member can be created.
T	Transformer tap setting.
u	Set of independent and control variables.
V_G	Voltage magnitude at the generation bus.
V_i	Voltage magnitude at buses i .
V_L	Voltage magnitudes at the load bus.
x	Set of dependent/state variables.
$X_{j,\text{mut}}$	j^{th} control variable of a mutated member
$\alpha_i, \beta_i, \gamma_i, \omega_i, \mu_i$	Emission characteristics of the i^{th} generator.
α^k	Perturbation factor at k^{th} iteration.
θ_i	Voltage angles at buses i .
$\lambda_P, \lambda_Q, \lambda_V, \lambda_S$	Penalty coefficients for the inequality constraints.
μ_i	Normalized membership function value.
σ	Standard deviation operators.
\prec_n	Crowded-comparison operator.

REFERENCES

- [1] A. E. Chaib, H. R. E. H. Bouchekara, R. Mehasni, and M. A. Abido, “Optimal power flow with emission and non-smooth cost functions using backtracking search optimization algorithm,” *Int. J. Electr. Power Energy Syst.*, vol. 81, pp. 64–77, Oct. 2016, doi: [10.1016/j.ijepes.2016.02.004](https://doi.org/10.1016/j.ijepes.2016.02.004).
- [2] S. He, J. Y. Wen, E. Prempain, Q. H. Wu, J. Fitch, and S. Mann, “An improved particle swarm optimization for optimal power flow,” in *Proc. Int. Conf. Power Syst. Technol. (PowerCon)*, Nov. 2012, pp. 1–40, doi: [10.1109/icpst.2004.1460265](https://doi.org/10.1109/icpst.2004.1460265).
- [3] M. Ghasemi, S. Ghavidel, E. Akbari, and A. A. Vahed, “Solving nonlinear, non-smooth and non-convex optimal power flow problems using chaotic invasive weed optimization algorithms based on chaos,” *Energy*, vol. 73, pp. 340–353, Aug. 2014, doi: [10.1016/j.energy.2014.06.026](https://doi.org/10.1016/j.energy.2014.06.026).

- [4] M. Niu, C. Wan, and Z. Xu, "A review on applications of heuristic optimization algorithms for optimal power flow in modern power systems," *J. Mod. Power Syst. Clean Energy*, vol. 2, no. 4, pp. 289–297, Dec. 2014, doi: [10.1007/s40565-014-0089-4](https://doi.org/10.1007/s40565-014-0089-4).
- [5] J. Zhang, Q. Tang, P. Li, D. Deng, and Y. Chen, "A modified MOEA/D approach to the solution of multi-objective optimal power flow problem," *Appl. Soft Comput.*, vol. 47, pp. 494–514, Oct. 2016, doi: [10.1016/j.asoc.2016.06.022](https://doi.org/10.1016/j.asoc.2016.06.022).
- [6] H. Bouchekara, "Optimal power flow using black-hole-based optimization approach," *Appl. Soft Comput.*, vol. 24, pp. 879–888, Nov. 2014, doi: [10.1016/j.asoc.2014.08.056](https://doi.org/10.1016/j.asoc.2014.08.056).
- [7] M. Adaryani and A. Karami, "Artificial bee colony algorithm for solving multi-objective optimal power flow problem," *Int. J. Electr. Power Energy Syst.*, vol. 53, pp. 219–230, Dec. 2013, doi: [10.1016/j.ijepes.2013.04.021](https://doi.org/10.1016/j.ijepes.2013.04.021).
- [8] H. R. E. H. Bouchekara, A. E. Chaib, M. A. Abido, and R. A. El-Sehiemy, "Optimal power flow using an improved colliding bodies optimization algorithm," *Appl. Soft Comput.*, vol. 42, pp. 119–131, May 2016, doi: [10.1016/j.asoc.2016.01.041](https://doi.org/10.1016/j.asoc.2016.01.041).
- [9] V. Raviprabakaran and R. C. Subramanian, "Enhanced ant colony optimization to solve the optimal power flow with ecological emission," *Int. J. Syst. Assurance Eng. Manage.*, vol. 9, no. 1, pp. 58–65, Feb. 2018, doi: [10.1007/s13198-016-0471-x](https://doi.org/10.1007/s13198-016-0471-x).
- [10] A.-A. A. Mohamed, Y. S. Mohamed, A. A. M. El-Gaafary, and A. M. Hemeida, "Optimal power flow using moth swarm algorithm," *Electr. Power Syst. Res.*, vol. 142, pp. 190–206, Jan. 2017, doi: [10.1016/j.epsr.2016.09.025](https://doi.org/10.1016/j.epsr.2016.09.025).
- [11] K. Abaci and V. Yamacli, "Differential search algorithm for solving multi-objective optimal power flow problem," *Int. J. Electr. Power Energy Syst.*, vol. 79, pp. 1–10, Jul. 2016, doi: [10.1016/j.ijepes.2015.12.021](https://doi.org/10.1016/j.ijepes.2015.12.021).
- [12] P. P. Biswas, P. N. Suganthan, R. Mallipeddi, and G. A. J. Amaralatunga, "Optimal power flow solutions using differential evolution algorithm integrated with effective constraint handling techniques," *Eng. Appl. Artif. Intell.*, vol. 68, pp. 81–100, Feb. 2018, doi: [10.1016/j.engappai.2017.10.019](https://doi.org/10.1016/j.engappai.2017.10.019).
- [13] M. A. Taher, S. Kamel, F. Jurado, and M. Ebeed, "An improved moth-flame optimization algorithm for solving optimal power flow problem," *Int. Trans. Electr. Energy Syst.*, vol. 29, no. 3, Mar. 2019, Art. no. e2743, doi: [10.1002/etep.2743](https://doi.org/10.1002/etep.2743).
- [14] T. Niknam, M. R. Narimani, M. Jabbari, and A. R. Malekpour, "A modified shuffle frog leaping algorithm for multi-objective optimal power flow," *Energy*, vol. 36, no. 11, pp. 6420–6432, Nov. 2011, doi: [10.1016/j.energy.2011.09.027](https://doi.org/10.1016/j.energy.2011.09.027).
- [15] B. Mandal and P. K. Roy, "Multi-objective optimal power flow using quasi-oppositional teaching learning based optimization," *Appl. Soft Comput.*, vol. 21, pp. 590–606, Aug. 2014, doi: [10.1016/j.asoc.2014.04.010](https://doi.org/10.1016/j.asoc.2014.04.010).
- [16] A. Shabanpour-Haghghi, A. R. Seifi, and T. Niknam, "A modified teaching-learning based optimization for multi-objective optimal power flow problem," *Energy Convers. Manage.*, vol. 77, no. 1, pp. 597–607, 2014, doi: [10.1016/j.enconman.2013.09.028](https://doi.org/10.1016/j.enconman.2013.09.028).
- [17] N. Bilel, N. Mohamed, A. Zouhaier, and R. Lotfi, "An improved imperialist competitive algorithm for multi-objective optimization," *Eng. Optim.*, vol. 48, no. 11, pp. 1823–1844, Nov. 2016, doi: [10.1080/0305215X.2016.1141204](https://doi.org/10.1080/0305215X.2016.1141204).
- [18] D. Qin, Q. Sun, R. Wang, D. Ma, and M. Liu, "Adaptive bidirectional droop control for electric vehicles parking with vehicle-to-grid service in microgrid," *CSEE J. Power Energy Syst.*, vol. 6, no. 4, pp. 793–805, Dec. 2020, doi: [10.17775/CSEEPES.2020.00310](https://doi.org/10.17775/CSEEPES.2020.00310).
- [19] H. Chen, M. L. Bo, and Y. Zhu, "Multi-hive bee foraging algorithm for multi-objective optimal power flow considering the cost, loss, and emission," *Int. J. Electr. Power Energy Syst.*, vol. 60, pp. 203–220, Sep. 2014, doi: [10.1016/j.ijepes.2014.02.017](https://doi.org/10.1016/j.ijepes.2014.02.017).
- [20] J. Zhang, Q. Tang, P. Li, D. Deng, and Y. Chen, "A modified MOEA/D approach to the solution of multi-objective optimal power flow problem," *Appl. Soft Comput.*, vol. 47, pp. 494–514, Oct. 2016, doi: [10.1016/j.asoc.2016.06.022](https://doi.org/10.1016/j.asoc.2016.06.022).
- [21] M. Ghasemi, S. Ghavidel, M. M. Ghanbarian, and M. Gitizadeh, "Multi-objective optimal electric power planning in the power system using Gaussian bare-bones imperialist competitive algorithm," *Inf. Sci.*, vol. 294, pp. 286–304, Feb. 2015, doi: [10.1016/j.ins.2014.09.051](https://doi.org/10.1016/j.ins.2014.09.051).
- [22] H. Pulluri, R. Naresh, and V. Sharma, "An enhanced self-adaptive differential evolution based solution methodology for multiobjective optimal power flow," *Appl. Soft Comput.*, vol. 54, pp. 229–245, May 2017, doi: [10.1016/j.asoc.2017.01.030](https://doi.org/10.1016/j.asoc.2017.01.030).
- [23] X. Yuan, B. Zhang, P. Wang, J. Liang, Y. Yuan, Y. Huang, and X. Lei, "Multi-objective optimal power flow based on improved strength Pareto evolutionary algorithm," *Energy*, vol. 122, pp. 70–82, Mar. 2017, doi: [10.1016/j.energy.2017.01.071](https://doi.org/10.1016/j.energy.2017.01.071).
- [24] W. Warid, H. Hizam, N. Mariun, and N. I. A. Wahab, "A novel quasi-oppositional modified Jaya algorithm for multi-objective optimal power flow solution," *Appl. Soft Comput.*, vol. 65, pp. 360–373, Apr. 2018, doi: [10.1016/j.asoc.2018.01.039](https://doi.org/10.1016/j.asoc.2018.01.039).
- [25] G. Chen, X. Yi, Z. Zhang, and H. Wang, "Applications of multi-objective dimension-based firefly algorithm to optimize the power losses, emission, and cost in power systems," *Appl. Soft Comput.*, vol. 68, pp. 322–342, Jul. 2018, doi: [10.1016/j.asoc.2018.04.006](https://doi.org/10.1016/j.asoc.2018.04.006).
- [26] S. S. Reddy, "Optimal power flow using hybrid differential evolution and harmony search algorithm," *Int. J. Mach. Learn. Cybern.*, vol. 10, no. 5, pp. 1077–1091, May 2019, doi: [10.1007/s13042-018-0786-9](https://doi.org/10.1007/s13042-018-0786-9).
- [27] J. Zhang, S. Wang, Q. Tang, Y. Zhou, and T. Zeng, "An improved NSGA-III integrating adaptive elimination strategy to solution of many-objective optimal power flow problems," *Energy*, vol. 172, pp. 945–957, Apr. 2019, doi: [10.1016/j.energy.2019.02.009](https://doi.org/10.1016/j.energy.2019.02.009).
- [28] R. A. El Sehiemy, F. Selim, B. Bentouati, and M. A. Abido, "A novel multi-objective hybrid particle swarm and salp optimization algorithm for technical-economical-environmental operation in power systems," *Energy*, vol. 193, Feb. 2020, Art. no. 116817, doi: [10.1016/j.energy.2019.116817](https://doi.org/10.1016/j.energy.2019.116817).
- [29] P. P. Biswas, P. N. Suganthan, R. Mallipeddi, and G. A. J. Amaralatunga, "Multi-objective optimal power flow solutions using a constraint handling technique of evolutionary algorithms," *Soft Comput.*, vol. 24, no. 4, pp. 2999–3023, Feb. 2020, doi: [10.1007/s00500-019-04077-1](https://doi.org/10.1007/s00500-019-04077-1).
- [30] G. Chen, J. Qian, Z. Zhang, and S. Li, "Application of modified pigeon-inspired optimization algorithm and constraint-objective sorting rule on multi-objective optimal power flow problem," *Appl. Soft Comput.*, vol. 92, Jul. 2020, Art. no. 106321, doi: [10.1016/j.asoc.2020.106321](https://doi.org/10.1016/j.asoc.2020.106321).
- [31] J. Qian, P. Wang, C. Pu, and G. Chen, "Joint application of multi-object beetle antennae search algorithm and BAS-BP fuel cost forecast network on optimal active power dispatch problems," *Knowl.-Based Syst.*, vol. 226, Aug. 2021, Art. no. 107149, doi: [10.1016/j.knosys.2021.107149](https://doi.org/10.1016/j.knosys.2021.107149).
- [32] G. Chen, J. Qian, Z. Zhang, and Z. Sun, "Applications of novel hybrid bat algorithm with constrained Pareto fuzzy dominant rule on multi-objective optimal power flow problems," *IEEE Access*, vol. 7, pp. 52060–52084, 2019, doi: [10.1109/ACCESS.2019.2912643](https://doi.org/10.1109/ACCESS.2019.2912643).
- [33] G. Chen, J. Qian, Z. Zhang, and Z. Sun, "Multi-objective optimal power flow based on hybrid firefly-bat algorithm and constraints-prior object-fuzzy sorting strategy," *IEEE Access*, vol. 7, pp. 139726–139745, 2019, doi: [10.1109/ACCESS.2019.2943480](https://doi.org/10.1109/ACCESS.2019.2943480).
- [34] E. Naderi, M. Pourakbari-Kasmaei, F. V. Cerna, and M. Lehtonen, "A novel hybrid self-adaptive heuristic algorithm to handle single- and multi-objective optimal power flow problems," *Int. J. Electr. Power Energy Syst.*, vol. 125, Feb. 2021, Art. no. 106492, doi: [10.1016/j.ijepes.2020.106492](https://doi.org/10.1016/j.ijepes.2020.106492).
- [35] A. M. Shaheen, R. A. El-Sehiemy, M. M. Alharthi, S. S. M. Ghoneim, and A. R. Ginidi, "Multi-objective jellyfish search optimizer for efficient power system operation based on multi-dimensional OPF framework," *Energy*, vol. 237, Dec. 2021, Art. no. 121478, doi: [10.1016/j.energy.2021.121478](https://doi.org/10.1016/j.energy.2021.121478).
- [36] A. M. Shaheen, R. A. El-Sehiemy, H. M. Hasanien, and A. R. Ginidi, "An improved heap optimization algorithm for efficient energy management based optimal power flow model," *Energy*, vol. 250, Jul. 2022, Art. no. 123795, doi: [10.1016/j.energy.2022.123795](https://doi.org/10.1016/j.energy.2022.123795).
- [37] J. Qian, P. Wang, C. Pu, X. Peng, and G. Chen, "Application of modified beetle antennae search algorithm and BP power flow prediction model on multi-objective optimal active power dispatch," *Appl. Soft Comput.*, vol. 113, Dec. 2021, Art. no. 108027, doi: [10.1016/j.asoc.2021.108027](https://doi.org/10.1016/j.asoc.2021.108027).
- [38] H. T. Kahraman, M. Akbel, and S. Duman, "Optimization of optimal power flow problem using multi-objective manta ray foraging optimizer," *Appl. Soft Comput.*, vol. 116, Feb. 2022, Art. no. 108334, doi: [10.1016/j.asoc.2021.108334](https://doi.org/10.1016/j.asoc.2021.108334).
- [39] G. Chen, X. Yi, Z. Zhang, and H. Wang, "Applications of multi-objective dimension-based firefly algorithm to optimize the power losses, emission, and cost in power systems," *Appl. Soft Comput.*, vol. 68, pp. 322–342, Jul. 2018, doi: [10.1016/j.asoc.2018.04.006](https://doi.org/10.1016/j.asoc.2018.04.006).
- [40] M. A. Abido, "Environmental/economic power dispatch using multi-objective evolutionary algorithms," *IEEE Trans. Power Syst.*, vol. 18, no. 4, pp. 1529–1537, Nov. 2003, doi: [10.1109/TPWRS.2003.818693](https://doi.org/10.1109/TPWRS.2003.818693).

- [41] M. S. Gonçalves, R. H. Lopez, and L. F. F. Miguel, "Search group algorithm: A new Metaheuristic method for the optimization of truss structures," *Comput. Struct.*, vol. 153, pp. 165–184, Jun. 2015, doi: [10.1016/j.compstruc.2015.03.003](https://doi.org/10.1016/j.compstruc.2015.03.003).
- [42] D. E. Goldberg, *Genetic Algorithms in Search, Optimization and Machine Learning*, 1st ed. Reading, MA, USA: Addison-Wesley, 1989.
- [43] T. H. B. Huy, T. V. Tran, D. N. Vo, and H. T. T. Nguyen, "An improved Metaheuristic method for simultaneous network reconfiguration and distributed generation allocation," *Alexandria Eng. J.*, vol. 61, no. 10, pp. 8069–8088, Oct. 2022, doi: [10.1016/j.aej.2022.01.056](https://doi.org/10.1016/j.aej.2022.01.056).
- [44] K. Deb, A. Pratap, S. Agarwal, and T. Meyarivan, "A fast and elitist multiobjective genetic algorithm: NSGA-II," *IEEE Trans. Evol. Comput.*, vol. 6, no. 2, pp. 182–197, Apr. 2002, doi: [10.1109/4235.996017](https://doi.org/10.1109/4235.996017).
- [45] B.-H. Truong, P. Nallagownden, K. H. Truong, R. Kannan, D. N. Vo, and N. Ho, "Multi-objective search group algorithm for thermo-economic optimization of flat-plate solar collector," *Neural Comput. Appl.*, vol. 33, no. 19, pp. 12661–12687, Oct. 2021, doi: [10.1007/s00521-021-05915-w](https://doi.org/10.1007/s00521-021-05915-w).
- [46] S. Duman, U. Güvenç, Y. Sönmez, and N. Yörükere, "Optimal power flow using gravitational search algorithm," *Energ. Convers. Manage.*, vol. 59, no. 59, pp. 86–95, Jul. 2012, doi: [10.1016/j.enconman.2012.02.024](https://doi.org/10.1016/j.enconman.2012.02.024).
- [47] W. Sheng, K.-Y. Liu, Y. Liu, X. Meng, and Y. Li, "Optimal placement and sizing of distributed generation via an improved nondominated sorting genetic algorithm II," *IEEE Trans. Power Del.*, vol. 30, no. 2, pp. 569–578, Apr. 2015, doi: [10.1109/TPWRD.2014.2325938](https://doi.org/10.1109/TPWRD.2014.2325938).
- [48] O. Alsac and B. Stott, "Optimal load flow with steady-state security," *IEEE Trans. Power App. Syst.*, vol. PAS-93, no. 3, pp. 745–751, May 1974, doi: [10.1109/TPAS.1974.293972](https://doi.org/10.1109/TPAS.1974.293972).
- [49] R. D. Zimmerman and C. E. Murillo-Sánchez, *MATPOWER-Manual-4.1.pdf*. Ithaca, NY, USA: Cornell Univ., Power Systems Engineering Research Center, 2011. Accessed: Sep. 19, 2020. [Online]. Available: <https://matpower.org/docs/MATPOWER-manual-4.1.pdf>
- [50] A. M. Shaheen, R. A. El-Sehiemy, and S. M. Farrag, "Solving multi-objective optimal power flow problem via forced initialised differential evolution algorithm," *IET Gener. Transmiss. Distrib.*, vol. 10, no. 7, pp. 1634–1647, May 2016, doi: [10.1049/iet-gtd.2015.0892](https://doi.org/10.1049/iet-gtd.2015.0892).
- [51] S. Mirjalili, P. Jangir, and S. Saremi, "Multi-objective ant lion optimizer: A multi-objective optimization algorithm for solving engineering problems," *Appl. Intell.*, vol. 46, no. 1, pp. 79–95, Jan. 2017, doi: [10.1007/s10489-016-0825-8](https://doi.org/10.1007/s10489-016-0825-8).
- [52] S. Z. Mirjalili, S. Mirjalili, S. Saremi, H. Faris, and I. Aljarah, "Grasshopper optimization algorithm for multi-objective optimization problems," *Appl. Intell.*, vol. 48, no. 4, pp. 805–820, 2018, doi: [10.1007/s10489-017-1019-8](https://doi.org/10.1007/s10489-017-1019-8).
- [53] J. L. C. Pereira, G. A. Oliver, M. B. Francisco, S. S. Cunha, Jr., and G. F. Gomes, "Multi-objective lichtenberg algorithm: A hybrid physics-based meta-heuristic for solving engineering problems," *Expert Syst. Appl.*, vol. 187, Jan. 2022, Art. no. 115939, doi: [10.1016/j.eswa.2021.115939](https://doi.org/10.1016/j.eswa.2021.115939).
- [54] Y.-N. Wang, L.-H. Wu, and X.-F. Yuan, "Multi-objective self-adaptive differential evolution with elitist archive and crowding entropy-based diversity measure," *Soft Comput.*, vol. 14, no. 3, p. 193, Jan. 2009, doi: [10.1007/s00500-008-0394-9](https://doi.org/10.1007/s00500-008-0394-9).
- [55] K. Deb, *Multi-Objective Optimization Using Evolutionary Algorithms*. Hoboken, NJ, USA: Wiley, 2001.



TRUONG HOANG BAO HUY received the B.Eng. degree in electrical and electronics engineering from the Ho Chi Minh City University of Technology (HCMUT), VNU-HCM, Vietnam, in 2017, and the M.S. degree in electrical and electronics engineering from Universiti Teknologi Petronas (UTP), Malaysia, in 2020. He is currently pursuing the Ph.D. degree with the Department of Internet of Things, Soonchunhyang University, Asan, South Korea. His research interests include energy management, smart grids, microgrids, and artificial intelligence-based algorithms and their application in optimization problems.



DAEHEE KIM (Member, IEEE) received the B.S. degree in electrical and electronic engineering from Yonsei University, Seoul, South Korea, in 2003, and the M.S. and Ph.D. degrees in electrical and electronic engineering from Korea University, Seoul, in 2006 and 2016, respectively.

From 2006 to 2016, he was a Senior Engineer with Samsung Electronics, Suwon, South Korea, where he has conducted research on WiMAX and LTE systems. He is currently an Assistant Professor with the Department of Internet of Things, Soonchunhyang University, Asan, South Korea. His research interests include the Internet of Things, energy management, blockchain, 5G, and security for wireless networks.



DIEU NGOC VO received the B.Eng. and M.Eng. degrees in electrical engineering from the Ho Chi Minh City University of Technology (HCMUT), VNU-HCM, Ho Chi Minh, Vietnam, in 1995 and 2000, respectively, and the D.Eng. degree in energy from the Asian Institute of Technology (AIT), Pathum Thani, Thailand, in 2007. He is currently an Associate Professor with the Department of Power Systems, Faculty of Electrical and Electronic Engineering, HCMUT, VNU-HCM. His research interests include applications of AI in power system optimization, power system operation and control, power system analysis, and power systems under deregulation.

• • •